A&A manuscript no.
(will be inserted by hand later)

Your thesaurus codes are:
07(08.03.1; 08.03.4; 08.09.2 IRC +10216; 08.13.2; 08.16.4)

ASTRONOMY
AND
ASTROPHYSICS
27.4.1994

Theoretical spectra of circumstellar dust shells around carbon-rich Asymptotic Giant Branch stars

J.M. Winters[1], **C. Dominik**[1,2], **and E. Sedlmayr**[1]

[1] Technische Universität Berlin, Institut für Astronomie und Astrophysik, PN 8-1, Hardenbergstr. 36, D-10623 Berlin, Federal Republic of Germany
[2] NASA Ames Research Center, Moffett Field, CA 94035, U.S.A.

Recieved date; accepted date

Abstract. Realistic modelling of circumstellar dust shells around evolved stars has to include a physical treatment of the interaction among hydrodynamics, thermodynamics, radiative transfer, chemistry and dust formation and -growth. A self-consistent solution of this problem is presented in the case of stationary, spherical symmetric dust-driven winds. The resulting shell structure and the mass-loss rate are completely determined by the three fundamental stellar parameters stellar mass $M_\star$, stellar luminosity $L_\star$ and effective temperature $T_{\rm eff}$ and by the element abundances $\epsilon_{\rm i}$.
A detailed calculation of the transport coefficients of the dust component by means of the particle size distribution function and the solution of the non-grey radiative transfer problem provide realistic synthetic spectra of the dust shell models.
We discuss the dependence of the resulting spectra on the stellar parameters in terms of infrared two colour diagrams. Application of these model calculations to the prominent infrared object IRC +10216 yields best agreement with the observed spectrum and the visibility data at maximum light for the stellar parameters $M_\star = 0.7M_\odot$, $L_\star = 2.4 \cdot 10^4 L_\odot$, $T_\star = 2010$K and a carbon to oxygen ratio of $\epsilon_{\rm C}/\epsilon_{\rm O} = 1.40$, which corresponds to a mass-loss rate of $\dot{M} = 8 \cdot 10^{-5} M_\odot {\rm yr}^{-1}$. In this model only amorphous carbon grains are considered as the main opacity source.
From this model a distance to IRC +10216 of $d = 170$pc is deduced. The total mass contained in the circumstellar dust shell implies an initial main sequence mass of $M_{\rm ZAMS} \geq 1.3M_\odot$ for IRC +10216.

Key words: Stars: carbon – circumstellar matter – Stars: individual: IRC +10216 – Stars: mass-loss – Stars: AGB

1. Introduction

The extended shells of cool giant stars are well known to be places of copious dust formation accompanied by considerable mass-loss. This is indicated by the spectra of these objects, which show large infrared excesses and partly characteristic emission or absorption features attributed to the presence of solid particles in the circumstellar shell. The identification of the features implies the presence of silicate compounds in the shells of oxygen-rich stars (i.e. [C]/[O] < 1, M-stars) and of carbon compounds in the shells of carbon-rich stars (i.e. [C]/[O] > 1, C-stars). Identifications for these features are for example given in (Treffers & Cohen 1974; Goebel & Moseley 1985) and in (Léger & Puget 1984). A compilation of identifications is also given in Gail & Sedlmayr (1987a).

The observed widths of the molecular rotation lines (mainly of CO) which are also present in the spectra, indicate expansion velocities of the circumstellar shells in the range from 8 to 40 kms^{-1} (e.g. Knapp et al. 1982). By calculating theoretical profiles of the CO J=1–0 and J=2–1 rotational lines Knapp & Morris (1985) derive mass-loss rates for late-type M- and C-stars in the range of $\sim 10^{-7}$ up to some $10^{-4}\,{\rm M}_\odot{\rm yr}^{-1}$. Similar values for the mass-loss rates are obtained from submillimeter observations (e.g. Sopka et al. 1985) and, in the case of oxygen-rich stars, from fitting the 10μm silicate feature (Schutte & Tielens 1989).

These calculations, however, are based on parameterized models of the hydrodynamical and thermodynamical structure of the dust shell and, therefore, do not include a physical description of the mass-loss process.

Several mechanisms have been proposed which might be responsible for causing the mass-loss of late-type giants at different stages of their evolution (cf. the reviews by Holzer & MacGregor (1985) and by Lafon & Berruyer (1991)). These mechanisms comprise essentially i) the dissipation of energy and momentum of different kinds of waves (acoustic waves, Alfvén waves, shock waves) which may propagate through the atmospheres, ii) radiation pressure on dust grains with subsequent momentum transfer to the gas, and iii) the combined effect of these mechanisms, i.e. levitation of the atmosphere by wave dissipation and effective acceleration of the material by radiation pressure on dust.

The suggestion, that radiation pressure on dust grains alone might be sufficient for driving the outflow (Wickramasinghe et al. 1966; Kwok 1975; Gail & Sedlmayr 1987b (henceforth called Paper III)) is supported by the observations. In this case the momentum flux of the radiation field has to be related to the momentum flux of the outflowing material. The observations indicate, that in many dust-forming shells the momentum flux of the outflowing material is comparable to the

Send offprint requests to: J.M. Winters momentum flux of the radiation field (Jura 1983b, 1986a) and proportional to the UV dust optical depth in the circumstellar shell (Knapp 1986). This result confirms, that radiation pressure on dust grains plays a decisive role for the acceleration of the wind.

Detailed calculations of the hydrodynamical structure of stationary circumstellar dust shells (CDS) have been performed by several authors (e.g. Salpeter 1974; Lucy 1976; Menietti & Fix 1978; Berruyer & Frisch 1983; Kozasa et al. 1984; Gail & Sedlmayr 1985, Paper III), while time-dependent situations like Miras and long-period variables are considered e.g. in Bowen (1988) and in Fleischer et al. (1991, 1992).

Each of these works focuses on different aspects of dust forming stellar envelopes. The common conclusion is, however, that radiation pressure on dust alone is capable for driving an outflow having low terminal velocities and high mass-loss rates in agreement with the observations. In the time-dependent models, radiation pressure on dust is also a necessary ingredient for producing the observed high mass-loss rates ($\dot{M} \geq 10^{-7} M_{\odot}\mathrm{yr}^{-1}$).

The self-consistent approach of Paper III represents a major progress for the modelling of stationary dust-driven winds. In this paper it is shown that the solution of the wind problem is completely determined by the specification of the three fundamental stellar parameters *stellar mass* $M_{\star}$, *stellar luminosity* $L_{\star}$ and *effective temperature* T_{eff} and by the element abundances ϵ_i. The structure of the circumstellar shell, in particular the mass-loss rate is a result of the calculation. Due to the self-consistent treatment, the model parameters are closely connected via the model equations, and thus, any other set of independent parameters, e.g. $M_{\star}$, $L_{\star}$, and mass-loss rate $\dot{M}$ can be chosen. In this case the effective temperature T_{eff} is a result of the calculation. The choice of this latter set of model parameters avoids the ambiguous definition of a stellar temperature (cf. Baschek et al. 1991; Appendix) and additionally can be advantageous for a more direct comparison to the observable quantities.

Despite their self-consistency the models presented in Paper III suffer from severe assumptions:

- the radiative transfer is treated in a semi-analytical approximation (Lucy 1971, 1976),
- the coupling among radiation field and hydrodynamical and thermodynamical structure of the shell is described in the small particle limit for the transport coefficients of the dust component,
- the transport coefficients of the gas and the dust are replaced by frequency integrated mean values,
- the temperature structure is calculated from the total opacity of gas and dust together, considered as a single component.

In the case of optically thick dust shells the Lucy approximation is not valid, which may lead to an incorrect determination of the radiation field and, therefore, of the temperature structure. The grey approximation does, of course, not provide the synthetic spectra of the dust shell models and, therefore, does not allow a comparison to observed spectra.

It is the aim of this paper, to eliminate these shortcomings of Paper III in order to arrive at a more realistic description which allows a reliable quantitative comparison to the observations. For this purpose it is necessary

- to solve the angle and frequency dependent radiative transfer problem,
- to calculate realistic frequency dependent transport coefficients by means of the size distribution function of the dust grains,
- to treat gas and dust as separate phases for calculating their individual temperature structures.

These improvements yield a more realistic description of the coupling among the dust component and the hydrodynamical and thermodynamical structure of the shell and in particular provide for the first time realistic infrared spectra of the dust shell models. As the structure of the models is completely determined by the fundamental stellar parameters, the comparison between the calculated spectra and observed spectra of individual objects allows the determination of the stellar parameters of these objects. Since the luminosity is a physical parameter of our models, also the distance to the objects can be derived from calculated and observed spectra.

We start in Sect. 2 with a description of the physical problem that determines the structure of a dust forming circumstellar environment. Our basic assumptions as well as the range of parameters considered in this paper are given in Sect. 3. In Sect. 4 we describe the numerical method applied to solve the dust-driven wind problem. The effects of the grain size distribution function on the transport coefficients are discussed in Sect. 5.1. As a first application we compare in Sect. 5.2 the results of our model calculations with observed flux ratios in the frame of infrared two colour diagrams. This comparison demonstrates, that stationary, spherically symmetric models of dust-driven winds are appropriate to describe the characteristic far infrared (FIR) appearance of the CDS of highly evolved carbon-rich Asymptotic Giant Branch (AGB) stars.

In a second step we discuss in detail the results of one model calculation which are in close agreement with the observed fluxes and visibility data of the prototype carbon-rich infrared object IRC +10216. This model is fixed by a stellar mass of $0.7 M_{\odot}$, a luminosity of $2.4 \cdot 10^4 L_{\odot}$, a mass-loss rate of $8 \cdot 10^{-5} M_{\odot}\mathrm{yr}^{-1}$ and an overabundance of carbon to oxygen of 1.40. The optical properties of the dust grains are described by the complex refractive index of amorphous carbon. From this model a distance to IRC +10216 of 170pc is derived. We finish with our conclusions in Sect. 6. In the Appendix some remarks on the determination of stellar temperature and stellar radius in the case of a star, surrounded by an extended circumstellar shell are given.

2. Self-consistent modelling of dust forming circumstellar shells

Self-consistent modelling of a dust forming circumstellar shell requires the simultaneous treatment of the coupled system of hydrodynamics, thermodynamics, chemistry and dust formation and -growth. The problem of a classical dust-free stellar atmosphere is modified by the emergence of dust in three respects (cf. Sedlmayr & Winters 1991):

i) The chemistry has to provide the densities of the condensating species, besides its role for the determination of the local transport coefficients of the gas.

ii) From the densities of the dust-forming species, the formation of critical clusters (which act as seed nuclei for grain growth) as well as the growth of these clusters to macroscopic particles has to be described in detail. In order to determine the transport coefficients of the dust component, the local size distribution function of the dust particles has to be determined.

iii) Due to its huge opacity the dust controls the hydrodynamic and thermodynamic structure of the circumstellar shell. As the values for the transport coefficients of the dust, via the process of dust formation and growth, in turn depend sensitively on the local kinetic gas temperature and gas density, the emergence of dust in a stellar atmosphere introduces a strong, nonlinear coupling among the physical subsystems as depicted in Fig. 1.

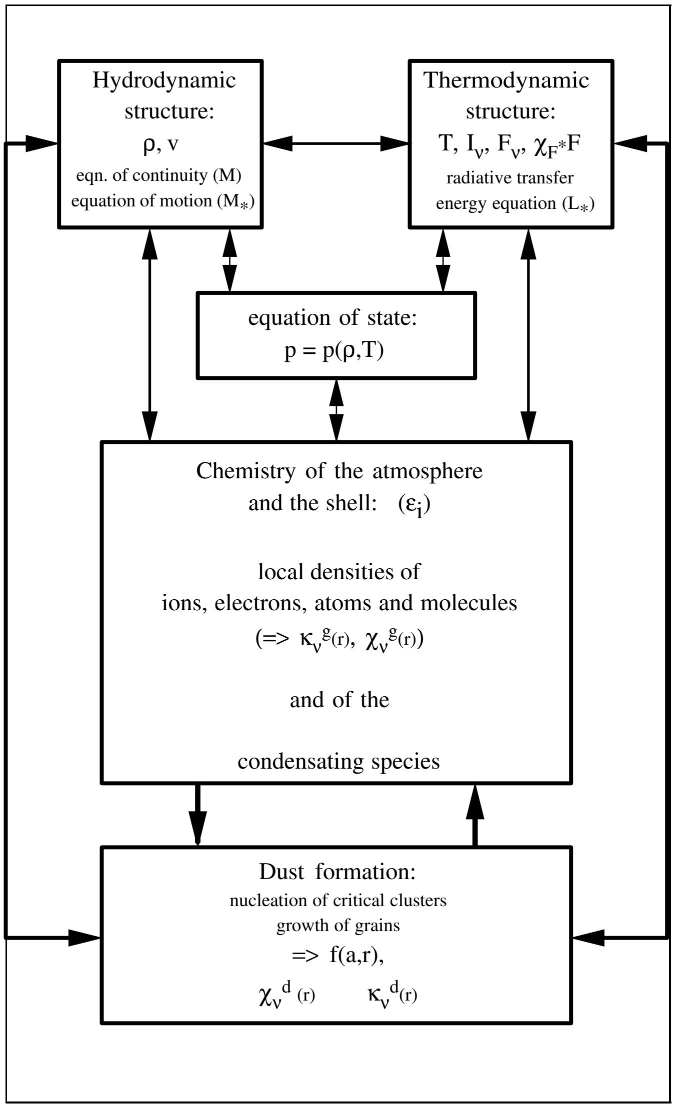

Fig. 1. The physical problem of a dust-driven wind

By consumption of the dust-forming species, dilution of the surrounding gas by accelerating an outflow and by thermal heating, the dust changes its surroundings and, thus, regulates the conditions of its own formation. The process of dust formation in a circumstellar environment, therefore, is an extremely fine-tuned self-regulating process.

The self-consistent solution of the dust-driven wind problem is completely determined if three stellar parameters: *stellar mass* $M_\star$, *stellar luminosity* $L_\star$, *mass-loss rate* $\dot{M}$ and the initial element abundances $\epsilon_{\rm i}$ are specified. From the basic equations, it is natural to consider the mass-loss rate as a parameter instead of the stellar temperature. Values for stellar temperature and stellar radius are obtained as a result of the model calculation (cf. Appendix).

3. Basic equations, assumptions and range of model parameters

As the basic equations describing the hydrodynamical structure of the wind, the formation and growth of dust particles and the molecular concentrations have been discussed in detail elsewhere (Paper III; Gail & Sedlmayr 1988; Dominik et al. 1990), we shortly summarize the basic assumptions and equations here and only describe the calculation of the transport coefficients of the dust grains, our treatment of the radiative transfer problem and the determination of the temperature structure in more detail.

Throughout this paper we assume spherical symmetry and stationarity of the circumstellar shell.

3.1. Hydrodynamics

We consider a purely dust-driven wind. This assumption excludes any effects of pulsation of the star such as levitation and heating of the atmosphere by dissipation of wave momentum and -energy. The forces considered in the equation of motion are the gradients of thermal- and radiation pressure and gravitation. We assume complete momentum coupling between gas molecules and dust grains. Thus, the grain–gas mixture is hydrodynamically treated as one component. The assumption of complete momentum coupling between gas and dust component is always justified in the regime of substantial mass–loss ($\dot{M} \geq 10^{-8} M_\odot$/yr), where purely dust–driven winds are possible. In a thorough investigation, Krüger et al. (1994) show, that in this case the dust grains always move with their (size–dependent) equilibrium drift velocity (which is of the order of the isothermal sound speed) relative to the gas. Thus, although the grains are not position coupled to the gas, they are in fact completely momentum coupled to the gas.
Neglecting the (small) equilibrium drift velocity of the grains, the equation of mass conservation yields

$$4\pi r^2 \rho v = \dot{M} \tag{1}$$

where the mass-loss rate $\dot{M}$ is considered as a model parameter (r = radial coordinate, ρ = mass density, v = flow velocity).

From momentum conservation the equation of motion is given by

$$v\frac{\partial v}{\partial r} = -\frac{1}{\rho}\frac{\partial p}{\partial r} - \frac{GM_\star}{r^2}(1-\alpha). \tag{2}$$

where the stellar mass $M_\star$ has to be fixed as model parameter (p = gas pressure, G = gravitation constant). The quantity α denotes the radiative acceleration in units of the local gravitational deceleration:

$$\alpha = \frac{L_\star}{4\pi c G M_\star}\frac{\chi_{\rm H}}{\rho} \tag{3}$$

where radiative equilibrium has been assumed. The stellar luminosity $L_\star$ has to be specified as a model parameter. The flux-mean extinction coefficient $\chi_{\rm H}$ is the sum of the flux-mean extinction coefficients of gas ($\chi_{\rm H}^{\rm g}$) and dust ($\chi_{\rm H}^{\rm d}$), respectively (c = speed of light).

3.2. Thermodynamics

Regarding the thermodynamical structure of the dust envelope, we consider a multi–component system consisting of molecular gas and solid dust particles. The molecules, thermodynamically treated as one component, are assumed to be thermal emitters, characterized by the local gas–kinetic temperature $T^{\rm g}(r)$. The dust grains are assumed to be spherical particles obeying the local size distribution $f(a,r)$ where a denotes the grain radius. Each grain is assumed to be a thermal emitter, radiating according to its (size–dependent) internal lattice temperature $T^{\rm d}(a,r)$.

3.2.1. Transport coefficients of the dust grains

The transport coefficients of the dust grains contained in the size interval $(a, a+da)$ are defined by

$$\chi_\nu^{\rm d}(a,r)da = \pi a^2 Q^{\rm ext}(\nu,a) f(a,r) da \tag{4}$$

$$\kappa_\nu^{\rm sca,d}(a,r)da = \pi a^2 Q^{\rm sca}(\nu,a) f(a,r) da \tag{5}$$

$$\kappa_\nu^{\rm abs,d}(a,r)da = \chi_\nu^{\rm d}(a,r)da - \kappa_\nu^{\rm sca,d}(a,r)da \tag{6}$$

where $\chi_\nu^{\rm d}(a,r)da$ denotes the extinction coefficient, $\kappa_\nu^{\rm sca,d}(a,r)da$ the scattering coefficient and $\kappa_\nu^{\rm abs,d}(a,r)da$ the absorption coefficient of dust grains having radii in the interval $(a, a+da)$, respectively. In writing Eq. (5) we assume isotropic, coherent scattering of radiation by the dust grains. The extinction and scattering efficiencies $Q^{\rm ext}(\nu,a)$ and $Q^{\rm sca}(\nu,a)$ of a grain of radius a are calculated from Mie theory assuming homogeneous spherical particles with given complex refractive index (cf. Sect. 3.2.2).
As the grains are assumed to be thermal emitters, the radiation energy emitted by dust grains in the size interval $(a, a+da)$ is determined by

$$\epsilon_\nu^{\rm d}(a,r)da = \pi a^2 Q^{\rm abs}(\nu,a) B_\nu(T^{\rm d}(a,r)) f(a,r) da \tag{7}$$

where B_ν is the Kirchhoff–Planck function. The absorption efficiency $Q^{\rm abs}(\nu,a)$ follows from

$$Q^{\rm abs}(\nu,a) = Q^{\rm ext}(\nu,a) - Q^{\rm sca}(\nu,a)\ . \tag{8}$$

In order to apply Mie theory, we have to restrict the above equations (4) ...(7) to macroscopic particles, i.e. to grain sizes $a > a_\ell$. We choose a_ℓ in the order of $10^{-3}\,\mu$m which corresponds to a minimum number of $\approx 10^2 \ldots 10^3$ atoms contained in the smallest dust grains. The transport coefficients of the dust component in total, as they enter into the radiative transfer problem, are obtained by integrating the contributions of the individual size intervals over the range $a_\ell \le a < \infty$:

$$\chi_\nu^{\rm d}(r) = \int_{a_\ell}^{\infty} \chi_\nu^{\rm d}(a,r)da \tag{9}$$

$$\kappa_\nu^{\rm sca,d}(r) = \int_{a_\ell}^{\infty} \kappa_\nu^{\rm sca,d}(a,r)da \tag{10}$$

$$\kappa_\nu^{\rm abs,d}(r) = \int_{a_\ell}^{\infty} \kappa_\nu^{\rm abs,d}(a,r)da \tag{11}$$

$$\epsilon_\nu^{\rm d}(r) = \int_{a_\ell}^{\infty} \epsilon_\nu^{\rm d}(a,r)da \tag{12}$$

3.2.2. Optical properties of the grains

For calculating the extinction and scattering efficiencies $Q^{\rm ext}(\nu,a)$ and $Q^{\rm sca}(\nu,a)$ of the dust grains, the optical properties of the grain material, described by its complex refractive index $m(\nu)$, have to be specified. In this paper we consider the formation of pure carbon grains, i.e. we do not attempt to model the dust features which might be present in the spectra of C-stars (eg. SiC, Treffers & Cohen 1974; MgS, Goebel & Moseley 1985).

The optical constants of the grains not only depend on the dust material but also on the microscopic structure (crystalline or amorphous) of the particles. Both modifications are possible in the case of carbon grains. As the internal structure of the grains formed in the circumstellar environment is not known a priori, in principle both types have to be considered here. Recent spectral modelling (eg. Jura 1983a, 1986a; Sopka et al. 1985; Martin & Rogers 1987; Orofino et al. 1990), however, implies the presence of amorphous grains rather than graphite particles in the circumstellar shells around C-stars. This is consistent with physical considerations, predicting the formation of inhomogeneous grains with crystalline cores surrounded by amorphous mantles which interact with the radiation field (Gail & Sedlmayr 1984).

The models presented in this paper, therefore, are calculated for amorphous carbon grains, the complex refractive index of which is taken from Maron (1990).

3.2.3. Transport coefficients of the gas

While the transport coefficients of the dust grains are treated in some detail in this paper, we represent the gas opacity only by its Rosseland-mean absorption coefficient. Thus, light scattering by the molecules is neglected and the frequency dependence of the gas opacity is not explicitly taken into account.

The total extinction coefficient χ_ν resulting from the gas and the dust component together

$$\chi_\nu(r) = \chi_\nu^{\rm g}(r) + \chi_\nu^{\rm d}(r) = \kappa_\nu^{\rm abs,g}(r) + \kappa_\nu^{\rm sca,g}(r) + \chi_\nu^{\rm d}(r) \tag{13}$$

is, thus, replaced by

$$\chi_\nu(r) = \kappa_{\rm R}^{\rm abs,g}(r) + \chi_\nu^{\rm d}(r) \tag{14}$$

in the present calculations. $\kappa_{\rm R}^{\rm abs,g}$ is the Rosseland-mean absorption coefficient of the gas, which is interpolated from tables kindly provided by M. Scholz.

3.2.4. Radiative transfer

With the assumptions stated in Sects. 3.2.1 and 3.2.3 the source function of the radiation field is given by

$$S_\nu(r) = \frac{\kappa_\nu^{\rm sca,d}(r)}{\chi_\nu(r)} J_\nu(r) + \frac{\kappa_{\rm R}^{\rm abs,g}(r)}{\chi_\nu(r)} B_\nu(T^{\rm g}(r)) + \frac{\epsilon_\nu^{\rm d}(r)}{\chi_\nu(r)} \tag{15}$$

where J_ν is the monochromatic mean intensity of the radiation field.

With the source function Eq. (15) we solve the stationary, spherically symmetric radiative transfer equation by means of iteration between i) the solution of the moment equations for the monochromatic mean intensity and ii) the formal solution for the monochromatic specific intensity along the characteristic paths of the partial differential equation. The system of moment equations is closed by the variable Eddington factor.

As boundary conditions we assume that at the inner boundary $r = R_0$, where the diffusion approximation is applied, the total radiative flux entering the atmosphere equals $L_\star/16\pi^2$ and that at the outer boundary at $r = R_{\rm max}$ no inwards flowing radiation exists. For details of this method we refer to Mihalas (1978).

3.2.5. Temperature stratification

For calculating the temperature structure of the dust envelope, we consider energy transport by radiation only. Due to the low densities (less than $10^{-10}\,{\rm g\,cm^{-3}}$), convective energy transport is inefficient and, thus, is neglected in the circumstellar shell. As we do not consider any energy release in the atmosphere due to dissipation of waves, the energy exchange can only be given by radiative gain and loss processes and by collisions between particles characterized by different temperatures. For calculating the gas temperature only the Rosseland-mean absorption coefficients of the gas phase have been available. Thus, the gas phase is thermodynamically treated as one component described by a single LTE temperature. Grain–grain collisions can be neglected due to the low particle density of the dust grains ($n^{\rm d} < 1{\rm cm}^{-3}$). Grain–gas collisions do not affect the temperature of the grain (cf. Appendix D in Gauger et al. 1990) but could be important for the gas temperature. However, the net energy gain or loss of the gas by this process critically depends on the coupling of the gas to the radiation field. As this coupling is severely underestimated by the Rosseland-mean opacities, we do not consider this process here (cf. Krüger et al. (1994) for a detailed discussion of this point). Thus, the energy gain and loss processes considered are absorption and thermal emission of radiation by the gas in grey approximation and frequency-dependent absorption and thermal emission by the dust grains. Hence, we assume radiative equilibrium for the gas component and the dust grains separately. The gas temperature is given by

$$T^{\rm g}(r) = \left[\frac{\pi}{\sigma}\frac{\kappa_{\rm J}^{\rm abs,g}(r)}{\kappa_{\rm P}^{\rm abs,g}(r)}J(r)\right]^{1/4} \tag{16}$$

where $\kappa_{\rm J}^{\rm abs,g}$ and $\kappa_{\rm P}^{\rm abs,g}$ denote the absorption-mean and Planck-mean absorption coefficient of the gas, respectively, J is the frequency integrated mean intensity of the radiation field and σ the Stefan–Boltzmann constant. With the present approximate treatment of the gas opacity, which means that

$$\kappa_{\rm J}^{\rm abs,g}(r) = \kappa_{\rm P}^{\rm abs,g}(r) = \kappa_{\rm R}^{\rm abs,g}(r)\ , \tag{17}$$

Eq. (16) reduces to

$$T^{\rm g}(r) = \left[\frac{\pi}{\sigma}J(r)\right]^{1/4}\ . \tag{18}$$

Assuming radiative equilibrium for each grain size a, the temperature of the grains is given by

$$T^{\rm d}(a,r) = \left[\frac{\pi}{\sigma}\frac{Q_{\rm J}^{\rm abs}(a)}{Q_{\rm P}^{\rm abs}(a)}J(r)\right]^{1/4}\ . \tag{19}$$

$Q_{\rm J}^{\rm abs}(a)$ and $Q_{\rm P}^{\rm abs}(a)$ are the absorption-mean and Planck-mean values of the absorption efficiency of the dust particles, respectively. In case of a size independent dust temperature, Eq. (19) transforms to

$$T^{\rm d}(r) = \left[\frac{\pi}{\sigma}\frac{\kappa_{\rm J}^{\rm abs,d}(r)}{\kappa_{\rm P}^{\rm abs,d}(r)}J(r)\right]^{1/4}\ . \tag{20}$$

For the numerical determination of the temperature stratification we apply the Unsöld–Lucy procedure, modified for spherical geometry.

3.3. Equation of state

The equation of state of the diluted gas is assumed to be the ideal gas law

$$p = \frac{\rho}{\mu}kT^{\rm g}\ . \tag{21}$$

The mean molecular mass μ is calculated from the dominant species H, H_2 and He (k = Boltzmann constant).

3.4. Chemistry

The molecular composition of the gas is important for two aspects of the model calculation:

i) The chemical structure determines the gas opacity. In this paper we describe the opacity of the gas by the Rosseland-mean absorption coefficient which is interpolated from tables given in the p-T plane. These opacity tables follow from chemical equilibrium calculations for C-rich compositions containing 95 species (Scholz & Tsuji 1984).

ii) The concentrations of the species which contribute to dust formation and growth have to be known. These are essentially C_2H, C_2H_2, and C_3H, the densities of which are calculated from a reduced equilibrium chemistry including only 7 species (cf. Dominik et al. 1990).

The initial element composition of the gas is assumed to be solar (Allen 1973) with the exception of the carbon abundance $\epsilon_{\rm C}$, which is considered as a parameter in order to account for a C-rich mixture.

The assumption of chemical equilibrium is justified in all situations where the expansion velocity is small and ionizing photons (e.g. from a chromosphere or the interstellar radiation field) are absent (Beck et al. 1992). The observations indicate, that dust forming cool giants, which are considered in this paper, generally do not possess chromospheres (Jura 1986b). Furthermore, interstellar UV photons cannot penetrate into the inner region of the dust shell (Mamon et al. 1988) and, thus, do not reach the region where the grains are formed. Photoreactions, therefore, can be neglected in the dust formation region. In a stationary dust-driven wind the velocity field is only produced by radiation pressure on dust. In the region where effective dust formation and - growth takes place, the velocity is small. Hence, dilution effects on the chemical timescales, which would cause deviations from the kinetic equilibrium, are negligible in the inner region of the shell and thus do not affect the concentrations of the dust forming species.

For a quantitative interpretation of molecular lines, however, which are formed in the outer shell regions, chemical non-equilibrium of course has to be considered in order to obtain reliable results e.g. for the column densities of these molecular species.

3.5. Grain nucleation and growth

We describe the condensation of carbon grains by classical nucleation theory extended to heteromolecular, homogeneous growth of these particles according to Gail et al. (1984) and Gail & Sedlmayr (1988). This theory is appropriate to describe the formation of amorphous carbon clusters but cannot account for large polyaromatic molecules which also might form in the circumstellar environment (Keller & Sedlmayr 1983; Keller 1987). As the observations seem to be compatible with the emergence of the amorphous component, this treatment of the dust formation process should be justified at least for the spectral modelling of the dust shell.

For the determination of the transport coefficients of the dust grains, the local grain-size distribution function is required. Since the distribution function is a result of the grain formation and -growth process, which in turn depends critically on the hydrodynamical and thermodynamical conditions in the dust forming medium, which again are essentially determined by the local transport coefficients, the determination of $f(a,r)$ represents a highly nonlinear regulation problem. Thus, any reliable calculation of the dust extinction requires the simultaneous solution of the complete set of the basic equations describing the physical conditions in the dust forming medium (cf. Fig. 1). Dominik et al. (1989) have developed a method which for dust forming circumstellar shells allows the calculation of the local size distribution function by an integration along the flow–characteristic once the model equations are solved. We apply this method for calculating the particle size distribution function.

3.6. The range of parameters

For the calculations presented in this paper, we choose the stellar mass $M_\star$, stellar luminosity $L_\star$, and the mass-loss rate $\dot{M}$ as basic parameters. For the construction of a model we also have to specify the carbon abundance $\epsilon_{\rm C}$ as all other elements are assumed to have solar abundances.

- **stellar mass** $M_\star$: The total mass $M_{\rm tot}$ of a star surrounded by a circumstellar shell is the sum of the mass of the central star $M_\star$ (i.e. the mass contained inside the photosphere) and the mass contained in the circumstellar shell $M_{\rm CS}$. In this paper we consider cool C-giants, which according to their evolution are believed to be AGB objects. As these objects probably evolve into planetary nebulae with central star masses of $M_\star \geq 0.55 M_\odot$ (Schönberner 1983), the minimum value of $M_\star$ should be $0.55 M_\odot$. The total mass $M_{\rm tot}$, on the other hand, cannot exceed the initial mass $M_{\rm ZAMS}$ of the progenitor star when it was located at the main sequence. According to Barnbaum et al. (1991) the initial mass of carbon-rich AGB-stars may be as large as $4 M_\odot$. The mass of a carbon-rich AGB-star, therefore, is approximately confined to the range $0.55 M_\odot \leq M_\star < 4 M_\odot$. Since purely dust-driven winds are possible only during the final AGB phases, the objects under consideration already should have lost a considerable fraction of their initial mass during their evolution to the top of the AGB. For this reason, the models presented here refer to the lower region of the possible mass range: $0.6 M_\odot \leq M_\star \leq 1 M_\odot$.
- **stellar luminosity** $L_\star$: Due to considerable uncertainties in the distance determination, the luminosities of AGB-stars are not known very accurately from the observations. Current estimates for the luminosities of these stars range from $2 \cdot 10^3 L_\odot$ to $5 \cdot 10^4 L_\odot$ (cf. van der Veen & Rugers 1989 and references therein). In the case of a purely dust-driven wind a minimum Eddington–luminosity is required for driving the outflow (cf. Dominik et al. 1990). For the range of stellar masses considered here, the required minimum luminosities are $L_\star \geq 2 \cdot 10^4 L_\odot$. Thus, our models are calculated for $2 \cdot 10^4 L_\odot \leq L_\star \leq 5 \cdot 10^4 L_\odot$.
- **mass-loss rate** $\dot{M}$: The observations indicate that the mass-loss rates for dust forming AGB stars range from $\approx 10^{-7} M_\odot {\rm yr}^{-1}$ to $10^{-4} M_\odot {\rm yr}^{-1}$ (cf. Knapp & Morris 1985). Accordingly the adopted values for the mass-loss rates of our models cover the range from $10^{-6} M_\odot {\rm yr}^{-1}$ to $10^{-4} M_\odot {\rm yr}^{-1}$.
- **carbon abundance** $\epsilon_{\rm C}$: In order to describe a carbon-rich element mixture we choose $\epsilon_{\rm C}/\epsilon_{\rm O} > 1$. Essentially three investigations exist in the literature, which are concerned with the determination of the C/O ratio in the atmospheres of carbon-rich AGB-stars. Lambert et al. (1986) determine rather low values of the C/O–ratio between $1 \leq \epsilon_{\rm C}/\epsilon_{\rm O} \leq 1.6$ where most of their objects have $\epsilon_{\rm C}/\epsilon_{\rm O} < 1.2$. Gow (1977) on the other hand finds considerable higher values of $1 \leq \epsilon_{\rm C}/\epsilon_{\rm O} \leq 10$ with most of the objects from his sample having $1.3 \leq \epsilon_{\rm C}/\epsilon_{\rm O} \leq 4$. Finally, Frantsman & Eglitis (1988) derive a mean value of $\langle \epsilon_{\rm C}/\epsilon_{\rm O} \rangle = 1.7$ from their analysis. As our model calculations indicate an almost linear correlation between the carbon to oxygen ratio and the terminal velocity of the wind (Dominik et al. 1990; Fleischer et al. 1992), high C/O ratios lead to terminal velocities, which are much higher than observed and thus are excluded from our calculations. The models presented here are calculated for $1.2 \leq \epsilon_{\rm C}/\epsilon_{\rm O} \leq 2$.

4. Iterative solution of the dust-driven wind problem

We calculate a consistent model of the dust shell by means of iteration between the equations describing the hydrodynamical and chemical (including dust) structure of the shell and the equations describing the radiative transfer, energy balance and radiation pressure on the dust grains. The whole iteration cycle is sketched in Fig. 2.

The initial model for this iteration is computed essentially from the equation system discussed in Dominik et al. (1990), which includes some slight modifications compared to the equations given in Paper III. In this first model, the temperature structure of the dust shell is obtained from the grey Eddington approximation for the spherical case (Lucy 1971, 1976). The consistency requirement $T(R_\star) = T_\star$ yields a value for the stellar radius of the initial model which is henceforth referred to as R_0. For the construction of the initial model we calculate the radiation pressure from the large particle approximation in the inner part of the dust shell and from the small particle approximation in the outer region (with an appropriate interpolation between this two limiting cases). This procedure turned out to be necessary in order to achieve convergence of the iteration (cf. Sect. 5.1). In the initial model the flux-mean extinction coefficient of the gas-grain mixture is replaced by the Rosseland-mean absorption coefficient of the mixture. This initial model provides a first guess of the complete atmospheric structure, including the local size distribution function of the dust particles. In the following iteration steps we take the current size distribution function in order to compute frequency–dependent extinction– and scattering efficiencies of the dust grains from

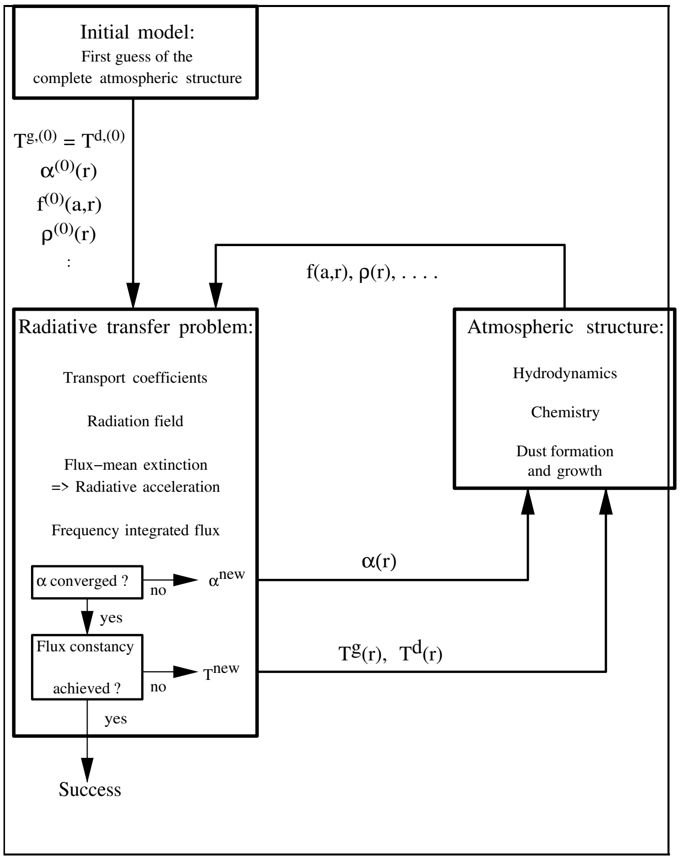

Fig. 2. Sketch of the global iterative scheme

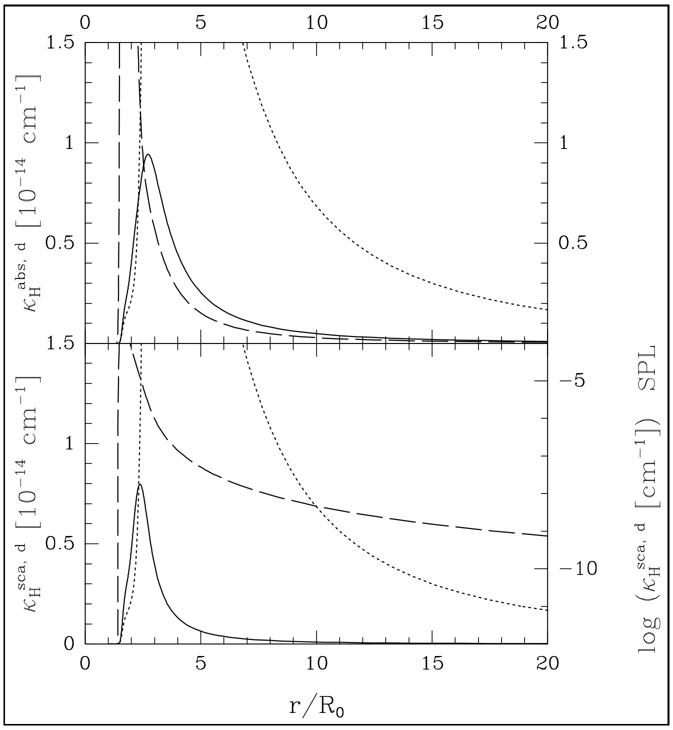

Fig. 3. Radial variation of the flux-mean absorption coefficient (upper diagram) and flux-mean scattering coefficient (lower diagram) of the dust component. The solid lines represent the values obtained from the size distribution function; the dotted lines refer to the large particle limit and the dashed lines show the small particle limit. In the lower diagram, the values of $\kappa_H^{sca,d}$ in the small particle limit (dashed line) are given by the ordinate at the r.h.s. on a logarithmic scale

Mie theory. With these improved transport coefficients we solve the radiative transfer problem and obtain an improved stratification of the radiative acceleration. If it deviates from the previous values of α, the atmospheric structure is recalculated with suitably improved values for the radiative acceleration and with the current temperature structure (both remain unchanged during the Newton-Raphson iteration within the "atmospheric structure block"). This inner cycle is repeated until α has converged. Then we check for flux-constancy and, if necessary, determine an improved temperature stratification which is subsequently used for recalculating the atmospheric structure.

Radiative acceleration as well as the temperature stratification are updated by applying automatically adjusted damping factors to the corrections which ensure numerical stability of the iterative process. A typical model takes some 300 iteration cycles until both, radiative acceleration and temperature stratification have converged.

5. Results and discussion

5.1. Grain extinction

The particle size distribution function produced in a stationary dust-driven wind is a power-law spectrum over a large interval of particle sizes: $f(a) \approx a^{-5}$ for $0.005\mu m < a < 10\mu m$ (Dominik et al. 1989). Thus, in particular in the inner region of the dust shell a relevant number of particles exist, which are large compared to the typical wavelength λ of the stellar radiation field. Therefore, the usual assumption of the small particle limit ($2\pi a \ll \lambda$) for calculating the transport coefficients of the dust grains is not justified. In order to demonstrate the errors introduced by the small particle approximation in the case of a stationary dust-driven wind, in Fig. 3 the resulting flux-mean values of the absorption and scattering coefficient, defined by

$$\kappa_H^{abs,d} = \frac{\int_0^\infty \kappa_\nu^{abs,d}\, H_\nu\, d\nu}{\int_0^\infty H_\nu\, d\nu} \tag{22}$$

$$\kappa_H^{sca,d} = \frac{\int_0^\infty \kappa_\nu^{sca,d}\, H_\nu\, d\nu}{\int_0^\infty H_\nu\, d\nu} \tag{23}$$

are compared with the results obtained from Eqs. (10) and (11) using the size distribution function. The parameters of this model are $M_\star = 0.7 M_\odot$, $L_\star = 2.4 \cdot 10^4 L_\odot$, $\epsilon_C/\epsilon_O = 1.40$ and $\dot{M} = 8 \cdot 10^{-5} M_\odot \mathrm{yr}^{-1}$ (cf. Sect. 5.5). The grains are assumed to consist of amorphous carbon with the complex refractive index taken from Maron (1990).

It can be seen from the upper diagram in Fig. 3 that in the outer parts of the dust shell ($r > 10R_0$) the small particle limit (dashed curve) yields a reasonable approximation of the absorption coefficient. In the innermost part of the shell, however, the absorption coefficient is well represented by the large particle limit ($2\pi a \gg \lambda$, dotted curve). Due to the relatively high gas density and the low expansion velocity in the region inside the sonic point ($r = r_s \simeq 2.2 R_0$), the dust grains formed grow under excellent conditions. This leads to the formation of large particles, which dominate in the inner region of the dust shell. The existence of these large particles is a specific result of the considered *stationary* wind: A gas element moves very slowly outwards in the region around the sonic point and, therefore, the dust particles contained in the element have much time to grow under favourable thermodynamical conditions (cf. Sect. 5.5.1).

From the lower diagram in Fig. 3 it can be seen, that in the innermost region the scattering coefficient is also closely approximated by the large particle limit. At no site in the atmosphere, however, scattering can be described in the small particle limit. Note, that the corresponding values of the small particle limit are given at the r.h.s. ordinate on a logarithmic scale. The values obtained for the scattering coefficient assuming the small particle limit deviate by orders of magnitude from the true values. This enormous effect is caused by the factor $(2\pi a/\lambda)^4$ in the expression for the small particle scattering efficiency where, in contradiction to the basic assumption, $2\pi a/\lambda$ is not small compared to unity in the relevant range of particle radii a and wavelengths λ.

Therefore, at least in cases where scattering is not negligible, it is necessary to calculate the transport coefficients from the exact expressions Eqs. (10) and (11) in order to obtain physically consistent results both for the radiative acceleration and the scattering optical depth and, thus, for the hydrodynamical structure of the wind and the emergent spectrum of the dust shell, respectively.

The main implication of the existence of large particles in the inner part of the dust shell is a considerable increase of the stellar luminosity required to accelerate the dust-driven wind: A necessary condition for dust driving is that the radiative acceleration of the material has to reach sufficiently high values inside the sonic point. Since particles large compared to the photon wavelength absorb radiation only proportional to their surface area (instead of proportional to the volume in the case of particles small compared to the wavelength) a correspondingly increased luminosity is required to surmount the Eddington limit for a dust-driven wind:

$$L_{\rm Edd} = \alpha_{\rm crit}\, 4\pi c G M_\star \left(\frac{\rho}{\chi_{\rm H}}\right) \tag{24}$$

where $\alpha_{\rm crit}$ is typically of the order of 0.7 at the sonic point.

5.2. Dependence of the model spectra on the stellar parameters

In order to investigate the dependence of the optical appearance of the dust shell models on the stellar parameters we have calculated a set of about 100 models for the parameters compiled in Tab. 1. We present our results in terms of the colour indices obtained from the FIR IRAS bands at 12μm, 25μm and 60μm (Fig. 4) and from the near infrared (NIF) standard photometric bands H ($\lambda_{\rm eff} = 1.65\mu$m), K ($\lambda_{\rm eff} = 2.2\mu$m) and L ($\lambda_{\rm eff} = 3.6\mu$m) (Fig. 5).

The crosses in Figs. 4 and 5 represent observed photometric fluxes of carbon-rich AGB-stars which are taken from Epchtein et al. (1990). In both figures, the observed colours of two particular objects are indicated by large open hexagons: in the (lower) left part of the diagrams the carbon Mira R For and in the (upper) right part the dust enshrouded C-star IRC +10216. The small filled symbols connected by lines of different type represent the model calculations. Along each line, one of the model parameters is varied while all other parameters are held constant. The model which is chosen as basis for the parameter variation (indicated by a filled triangle in both figures) is fixed by $M_\star = 0.7 M_\odot$, $L_\star = 3\cdot10^4 L_\odot$, $\dot M = 1\cdot10^{-4} M_\odot {\rm yr}^{-1}$ and $\epsilon_{\rm C}/\epsilon_{\rm O} = 1.40$.

Table 1. Range of model parameters

$M_\star/M_\odot$	L_4	$\dot M_{-4}$	$\epsilon_{\rm C}/\epsilon_{\rm O}$
0.6	$2.0-4.0$	$0.1-1.0$	1.4
0.7	$2.0-5.0$	$0.05-1.0$	$1.2-2.0$
0.8	$3.0-5.0$	$0.1-1.0$	1.4
0.9	$4.0-5.0$	$0.1-1.0$	1.4
1.0	$4.0-5.0$	$0.01-1.0$	$1.3-2.0$

$L_4 := L_\star/10^4 L_\odot$ $\quad$ $\dot M_{-4} := \dot M/10^{-4} M_\odot {\rm yr}^{-1}$

In case of the FIR colour indices (Fig. 4) the geometrical shell extension has a strong additional influence in particular on the ([25]-[60]) colour index in the sense, that an increasing shell extension shifts this colour index to larger values. This well known fact is indicated in Fig. 4 by the almost vertical dashed lines, each of which corresponds (from bottom to top) to an increasing value of $R_{\rm max}$. Thermal emission of cool dust, located at large distances from the central star, contributes significantly to the emergent flux at FIR wavelengths. The amount of thermally emitted radiation of course depends on the density in the outer shell region and, thus, on the mass-loss rate.

Along the solid lines the mass-loss rate increases from left to right ($5\cdot10^{-6} M_\odot yr^{-1}$, $1\cdot10^{-5} M_\odot yr^{-1}$, $5\cdot10^{-5} M_\odot yr^{-1}$, $1\cdot10^{-4} M_\odot yr^{-1}$). The upper solid line refers to a location of the outer shell boundary at $R_{\rm max} = 1\cdot10^4 R_0$, the middle solid line to $R_{\rm max} = 1\cdot10^3 R_0$ and the lowest to $R_{\rm max} = 5\cdot10^2 R_0$. It can be seen, that with increasing mass-loss rate the location of the outer boundary $R_{\rm max}$ has to be reduced accordingly in order to match the observed IRAS fluxes. This is due to the fact that the complete shell in the models is produced by a mass-loss rate which is constant with time. The phase of constant mass-loss rate, however cannot last for an arbitrary long time interval, the star would completely evaporate. In the real objects the mass-loss rate is believed to increase with time (cf. Dominik et al. 1990) and, therefore, the most extended parts of the shell have been produced in an evolutionary phase of the star when it had a smaller mass-loss rate. The mass density in the outer parts of the real shell, therefore, is lower than the density produced by the stationary wind models.

The dotted line indicates the effect of decreasing the stellar luminosity in steps of $5\cdot10^3 L_\odot$ from $5\cdot10^4 L_\odot$ (on the left) to $2.5\cdot10^4 L_\odot$ (on the right). Lower luminosities produce “cooler” shell spectra which is of course partly due to the corresponding reduction of the stellar temperature but is also due to a larger amount of dust produced in the models with decreased luminosity (cf. Sect. 5.3).

Along the short-dashed line the overabundance of carbon to oxygen $\epsilon_{\rm C}/\epsilon_{\rm O}$ is increased in steps of 0.1 from a value of 1.2 at the left to $\epsilon_{\rm C}/\epsilon_{\rm O} = 2$ at the right. The reddening of the spectra by the increased carbon abundance is a pure effect of the increased amount of dust, the stellar temperature remains

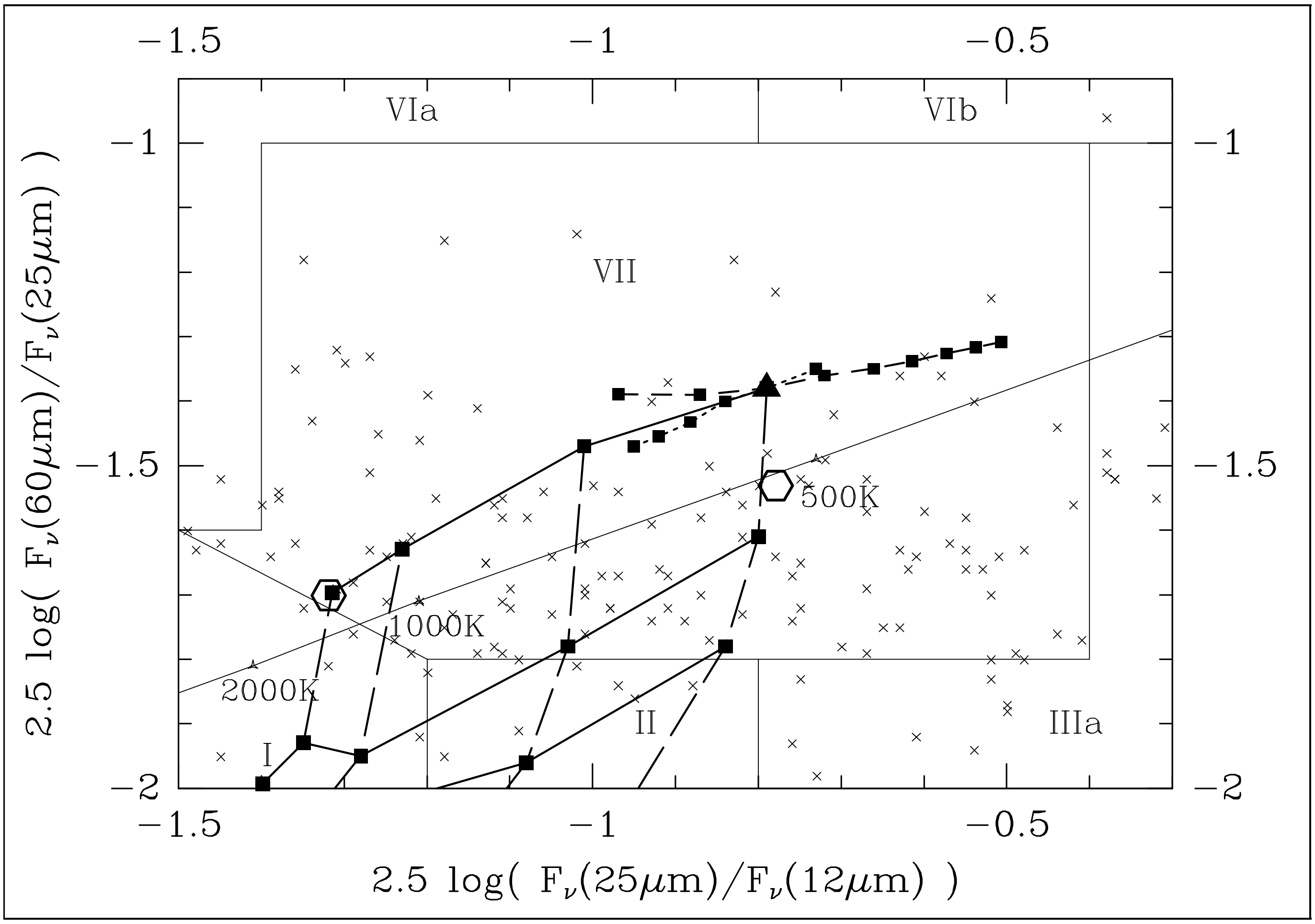

Fig. 4. IRAS two colour diagram. The roman numbered regions refer to the classification of van der Veen & Habing (1988). Crosses are observed values taken from Epchtein et al. (1990). The diagonal line connects black-body spectra at the indicated temperatures. The large open hexagons indicate the locations of IRC +10216 (right hexagon) and R For (left hexagon), the other symbols represent the model calculations (see text)

almost constant (between 2054K and 2040K) along this line. All models shown in Figs. 4 and 5 refer to a stellar mass of $M_\star = 0.7 M_\odot$. Within the range of masses considered (cf. Tab. 1), the model spectra are almost independent of mass.

From Fig. 4 it can be seen that self-consistent models of stationary, dust-driven winds are capable to reproduce the observed FIR fluxes of evolved carbon-rich circumstellar dust shells which are believed to mainly populate region VII of the IRAS two colour diagram (cf. van der Veen & Habing 1988).

In the NIF region (Fig. 5) the theoretical colour indices resulting from the self-consistent stationary wind models deviate in a systematic way from the corresponding observed values. Both, the observations and the calculations show an almost linear correlation between the $(\mathrm{H}\text{-}\mathrm{K})_0$ and $(\mathrm{K}\text{-}\mathrm{L})_0$ colour index, but with different gradients. The filled squares connected by lines of different type, which represent the calculations, are again obtained from varying the model parameters in the same way as described above. Solid line: mass-loss rate increases from left ($5 \cdot 10^{-6} M_\odot \mathrm{yr}^{-1}$) to right ($1 \cdot 10^{-4} M_\odot \mathrm{yr}^{-1}$); dashed line: carbon to oxygen ratio increases from left ($\epsilon_\mathrm{C}/\epsilon_\mathrm{O} = 1.2$) to right ($\epsilon_\mathrm{C}/\epsilon_\mathrm{O} = 2$); dotted line: luminosity decreases from left ($L_\star = 5 \cdot 10^4 L_\odot$) to right ($L_\star = 2.5 \cdot 10^4 L_\odot$). Obviously, none of them affects the gradient of the theoretical colour index correlation. In all models located below the black-body line, the transport coefficients are calculated from Eqs. (9) and (10), taking into account the particle size distribution function. Above the black-body line, five filled squares are shown at the border of the observed colours. These theoretical colour indices are obtained from model calculations, where the small particle limit has been assumed for calculating the dust opacity, although this assumption is not justified in a stationary dust-driven wind (cf. Sect. 5.1). A possible reason for this discrepancy between calculated and observed NIF colours might be the fact, that almost all objects which possess circumstellar dust shells are pulsating variables (Miras or long–period variables) (Habing 1990). Due to the periodic passage of shocks through the atmosphere, the time available for the dust grains to grow under favourable thermodynamical conditions is at least limited by the pulsation period of the star which is typically of the order of one year. Time-dependent model calculations of dust-forming circumstellar shells around long–period variables (Fleischer et al. 1992) in fact yield narrow grain-size distribution functions with a mean particle radius of

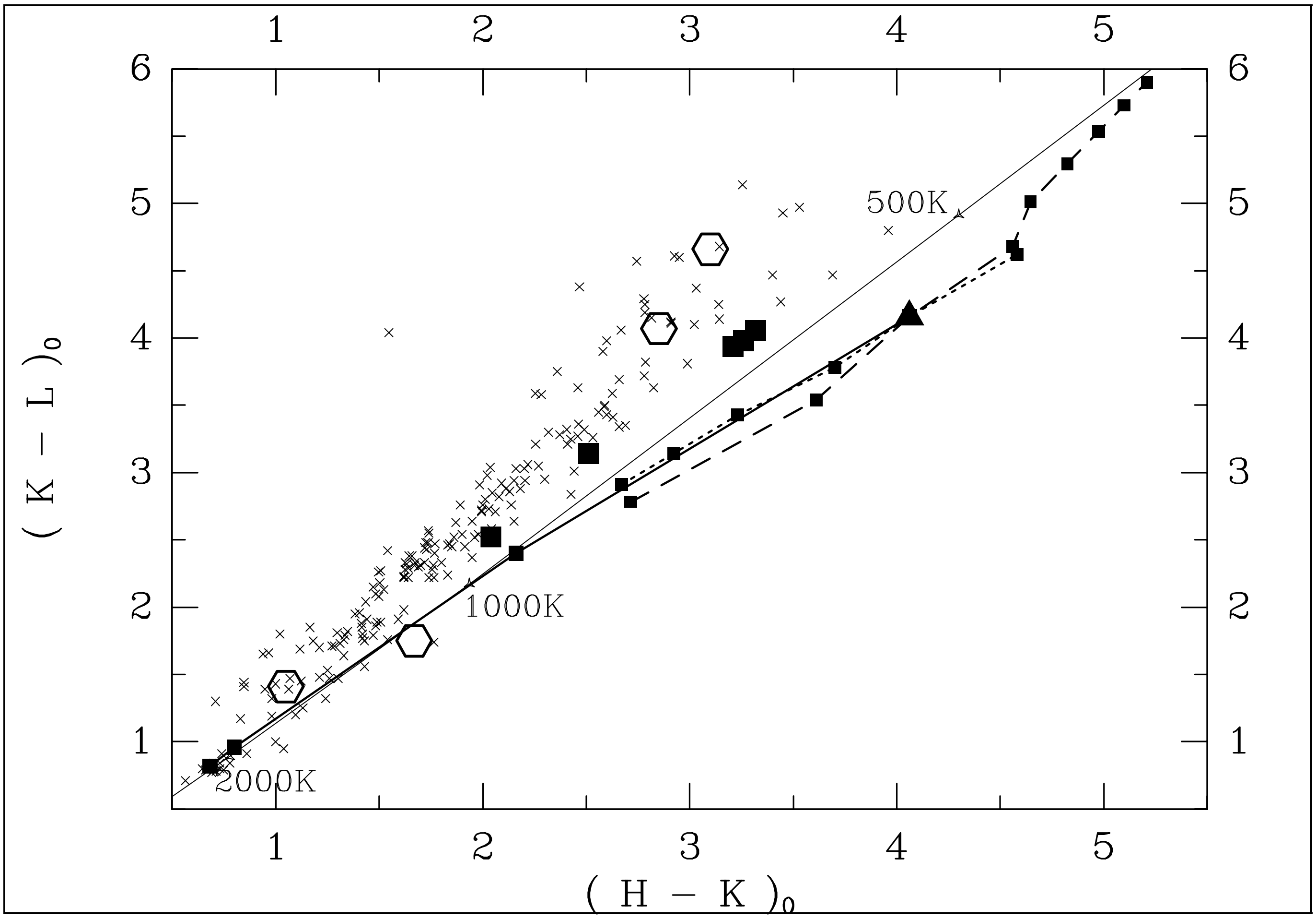

Fig. 5. Near infrared two colour diagram. Crosses represent observed colours taken from Epchtein et al. (1990), the diagonal line connects black-body spectra at the indicated temperatures. The large open hexagons represent the locations of IRC +10216 (upper right) and R For (lower left) at different phases of the light curve. Right and left symbol in each case correspond to light minimum and light maximum, respectively. The other symbols represent the model calculations (see text)

$r_{\rm m} \leq 0.1\mu$m throughout the circumstellar shell. These particles are small compared to the NIF wavelengths considered in Fig. 5. The theoretical spectra of these time-dependent models will be discussed in a subsequent paper.

5.3. Dependence of the models on the stellar parameters

In this section we describe the reaction of the dust shell model to variations of each of the model parameters. As the considered dust-driven wind represents the solution of a nonlinear physical problem (cf. Fig. 1), the variation of the model parameters affects the complete dust forming system in an intricate way. The main coupling among the different physical subsystems is governed by the dust opacity, which is roughly (in the small particle limit exactly) proportional to the amount of material condensed into grains. It is therefore advantageous, to discuss the dependence of the model structure on the stellar parameters in terms of the *degree of condensation* $f_{\rm cond}$, i.e. the ratio of actually condensed material to the amount of condensable material:

$$f_{\rm cond} = \frac{n_{\rm C,dust}}{(\epsilon_{\rm C} - \epsilon_{\rm O}) n_{<{\rm H}>}} \, . \tag{25}$$

Thereby we have assumed, that all oxygen is locked up in the CO molecule, which does not contribute to the formation of dust grains.

– Stellar mass $M_\star$: As long as a stationary dust-driven wind exists for a given set of stellar parameters, a variation of the stellar mass has only minor influence on both, the model structure and the shell spectrum. However, with $L_\star$ fixed, there exists an upper limit for the stellar mass above which pure dust driving is not sufficient to maintain the outflow. Therefore, the range of stellar masses for which stationary dust-driven winds exist is severely restricted for reasonable values of the stellar luminosity. An increase of the stellar mass results in somewhat lower wind velocities. This leads to a slight increase of the degree of condensation, caused by a more effective growth of the dust particles. The maximum value of α decreases almost linear with increasing mass of the central star (cf. Eq. (3)). Due to the larger degree of condensation the dust extinction reaches slightly higher values, an effect that results in slightly redder spectra. Simultaneously, the stellar temperature decreases ($\Delta T_\star \approx 200$K between $M_\star = 0.6 M_\odot$ and $M_\star = 1.0 M_\odot$) which also contributes to the “cooling” of the spectra.

- Stellar luminosity $L_\star$: By increasing the value of the stellar luminosity, the force acting on a *given* amount of dust increases. This leads to a steeper increase of the velocity in the region inside the sonic point, where effective dust condensation and growth takes place. Due to the corresponding faster dilution of the particle density in a co-moving gas element, the collision rates between dust particles and gas molecules decrease. Therefore, the dust grains grow less effectively, leading to smaller particles and a lower degree of condensation. The extinction coefficient remains smaller, leading to an almost unchanged value of the radiative acceleration (proportional to $L_\star \cdot \chi_{\rm H}/\rho$) and, thus, to a nearly unchanged terminal wind velocity. Due to the smaller dust opacity, the shell remains more transparent which, together with the simultaneously increased stellar temperature ($\Delta T_\star \approx 220$K between $L_\star = 2.5 \cdot 10^4 L_\odot$ and $L_\star = 5 \cdot 10^4 L_\odot$) leads to "hotter" spectra.
- Mass-loss rate $\dot{M}$: The main effect of increasing the mass-loss rate is, due to mass conservation, a corresponding increase of the local mass- and, thus, the local particle density. Therefore, the collision rates between dust particles and gas molecules increase with increasing $\dot{M}$, leading to a more efficient growth of the dust particles, which thus become larger, the degree of condensation increases. This results in higher values of the radiative acceleration outside the sonic point and a larger terminal wind velocity. Due to the increased dust opacity the shell spectrum becomes "cooler". Simultaneously the stellar temperature decreases by about 300K between $\dot{M} = 5 \cdot 10^{-6} M_\odot {\rm yr}^{-1}$ and $\dot{M} = 1 \cdot 10^{-4} M_\odot {\rm yr}^{-1}$.
- Carbon abundance $\epsilon_{\rm C}$: An increase of the carbon abundance directly increases the amount of condensable material $(\epsilon_{\rm C} - \epsilon_{\rm O}) n_{<H>}$. This results in an increase of the maximum value of the nucleation rate, i.e. more critical clusters are formed per second and unit volume. Therefore, a larger number of dust grains is formed, which increase the degree of condensation. The maximum value of α increases accordingly, and leads to a considerably increased terminal wind velocity. Thus, the collision rates decrease in a co-moving gas element, which results in a less effective growth of the particles. Consequently, the dust grains remain smaller at the end of the growth process. Due to the larger amount of dust (caused by the larger number of grains), the absorption of the short wavelength stellar radiation field becomes more efficient and, at the same time, more energy is thermally re-radiated by the dust grains in the FIR region. Thus, the spectra exhibit less flux in the visible and near infrared region and more flux in the FIR.

5.4. Dependence of the degree of condensation on the stellar parameters

The final degree of condensation reached in the CDS after the process of dust formation and growth has ceased is fixed by the model parameters and can be expressed as

$$f_{\rm cond} = \left(\frac{\dot{M}}{10^{-5} M_\odot {\rm yr}^{-1}} \right)^{0.78} \cdot \left(12.7\,(\epsilon_{\rm C}/\epsilon_{\rm O}) - 10.2 \log(\frac{L_\star}{L_\odot}) + 34.9 \right) \qquad (26)$$

which is obtained from a fit to the results of the numerical calculations. Equation (26) is correct within 20 % for the range of parameters given in Tab. 1. Within the range of stellar masses considered here ($0.6 M_\odot < M_\star < 1 M_\odot$) the degree of condensation is nearly independent of $M_\star$.

5.5. Model structure

In the following sections we discuss the structure and infrared appearance of a model characterized by the stellar parameters $M_\star = 0.7 M_\odot$, $L_\star = 2.4 \cdot 10^4 L_\odot$, $\dot{M} = 8 \cdot 10^{-5} M_\odot {\rm yr}^{-1}$ and a carbon to oxygen ratio of $\epsilon_{\rm C}/\epsilon_{\rm O} = 1.40$ This model yields a synthetic spectrum and spatial intensity distributions, that closely approximate the observed spectrum and visibilities of the carbon star IRC +10216 at maximum light (cf. Sects. 5.5.2 and 5.5.3). The terminal outflow velocity of 20.7 kms^{-1} resulting from this model calculation is significantly higher (about 6 kms^{-1}) than the respective value presently observed for IRC +10216 (13.7 kms^{-1} – 14.8 kms^{-1}, e.g. Olofsson et al. (1993)). This discrepancy is discussed in Sect. 5.5.4.

5.5.1. Radial structure

In Fig. 6 the radial structure of the dust shell model is shown. The formation of dust grains starts around $1.4 R_0$ ($R_0 = 9.25 \cdot 10^{13}$cm), which leads to a steep increase of the dust extinction $\chi_{\rm H}$ and, therefore, of the radiative force accelerating the dust grains. By momentum coupling of the grains to the surrounding gas, the momentum gained by the dust particles is transferred to the gas. This process results in an outward directed net acceleration ($\alpha > 1$ for $r > 2.25 R_0$) of the grain-gas mixture and, therefore, in an increasing outflow velocity v of the material. The transition from subsonic to supersonic motion occurs at $r = r_s = 2.2 R_0$ where α reaches a value of 0.75. Around $3 R_0$ the wind velocity exceeds the local escape velocity $v_{\rm esc}$. The atmospheric material, therefore, is lifted out of the stellar gravitational field within the first two stellar radii above the photosphere. The final outflow velocity of 20.7 kms^{-1} (cf. Sect. 5.5.4) is nearly reached at $20 R_0$. The material is essentially accelerated in the region between $2 R_0$ and $5\,R_0$. The gas temperature $T^{\rm g}$ in the region of effective dust formation and growth (around $r = 2.5 R_0$) is ≈ 1300K while the mass density in this region is about 10^{-14}gcm^{-3}. Thermal emission from the inner boundary of the dust envelope heats the gas inside the dust formation zone. The dust opacity leads to a substantial backwarming which results in an almost constant temperature throughout the region of effective dust formation. The size independent dust temperature $T^{\rm d}$ (cf. Eq. (20)) exceeds the (grey) gas temperature. The temperature difference produced by this greenhouse effect increases with increasing distance from the photosphere. The temperature difference between gas and dust reaches a maximum value of about 50K in this model.

Figure 7 displays the temperature structure for different grain sizes in the region of effective dust formation. The size independent dust temperature (dashed curve, computed from Eq. (20)) approaches the temperature of a small particle ($a = 0.01 \mu$m, upper dotted curve) within a narrow transition region around the sonic point between $2 R_0$ and $\approx 2.5 R_0$. The temperature of a large particle ($a = 10 \mu$m, lower dotted curve), which is the grey temperature ($Q(\nu) = {\rm const}_\nu$), is also shown in Fig. 7. The intermediate case ($a = 1 \mu$m) is indicated by the

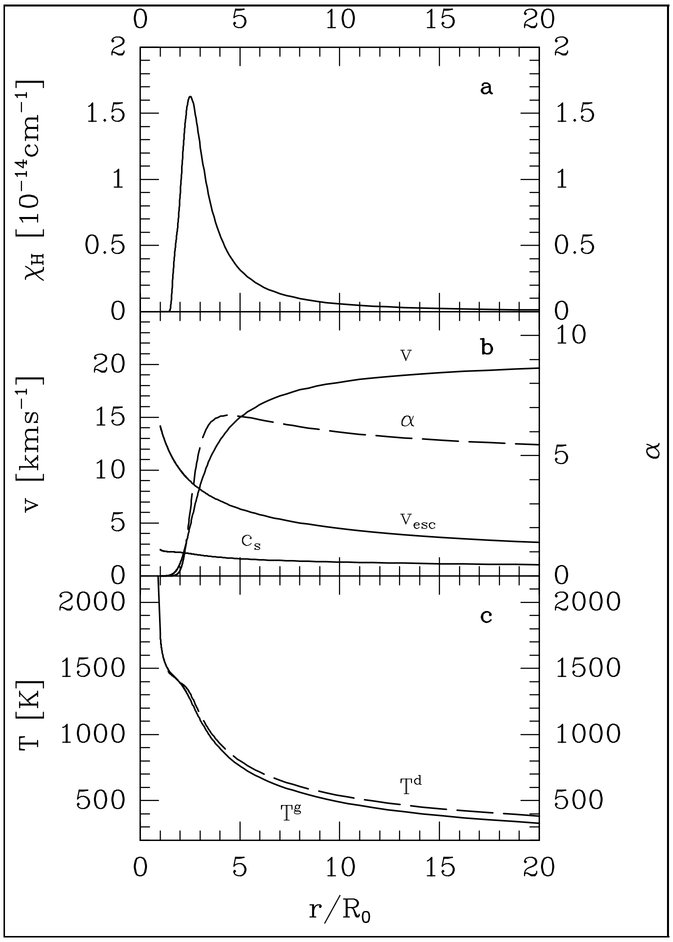

Fig. 6. Radial structure of the dust shell: **a** flux-mean extinction coefficient of the dust component, **b** hydrodynamic velocity v, local escape velocity v_{esc} and velocity of sound c_s (solid curves, l.h.s. ordinate) and radiative acceleration in units of the local gravitational deceleration α (dashed curve, r.h.s. ordinate), **c** gas temperature (solid line) and size-independent dust temperature (dashed line)

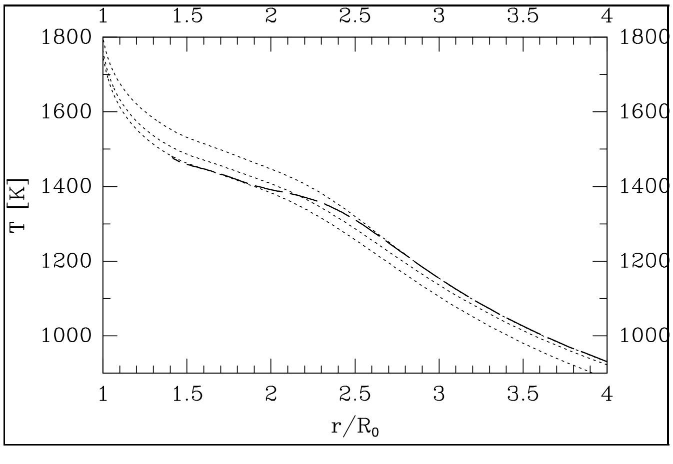

Fig. 7. Temperature structure for different grain sizes in the region around the sonic point. Upper dotted curve: particle radius $a = 0.01\mu$m, middle dotted curve $a = 1\mu$m, lower dotted curve $a = 10\mu$m, dashed curve: size independent dust temperature

middle dotted curve. This particle is large compared to the typical wavelength of the stellar radiation field (the maximum of $J_\nu(R_0)$ occurs at 2.5μm) but, concerning the temperature, becomes a small particle at distances $r > 4R_0$ (the maximum of $J_\nu(r > 4R_0)$ is reached at $\lambda > 4.7\mu$m). Thus, the small particle approximation is appropriate for calculating the temperature of the dust component outside the sonic point.

5.5.2. Emergent spectrum

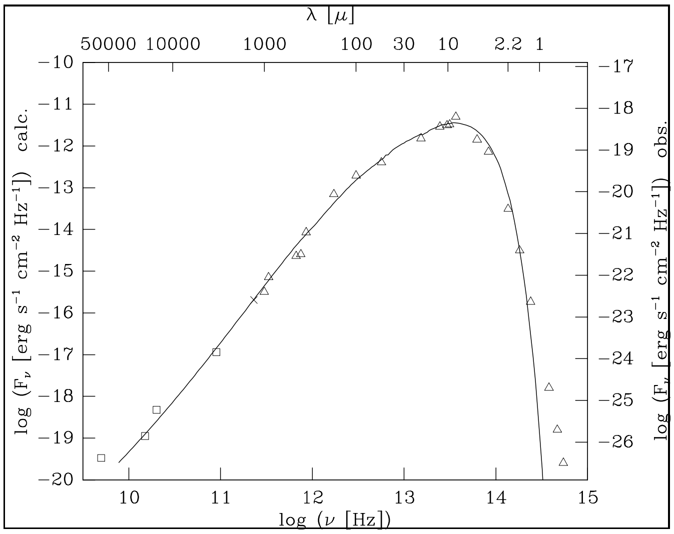

Fig. 8. Emergent spectrum of the dust shell model described in the text (solid line). The observational data for IRC +10216 are taken from Le Bertre (1987) and references therein (△), Sahai et al. (1989) (□) and Walmsley et al. (1991) (×)

In Fig. 8 the energy distribution produced by this dust shell model is shown together with observed photometric data of the C-rich infrared object IRC +10216. This source is known to be variable with a period of ~ 640d (Witteborn et al. 1980; Ridgway & Keady 1988). The symbols shown in Figs. 8 and 9 represent fluxes measured near the maximum of the 2.2μm light curve. The calculated spectrum shown in Fig. 8 results from assuming amorphous carbon described by the complex refractive index tabulated in Maron (1990). The outer boundary of the dust shell model is located at $2 \cdot 10^3 R_0$ which corresponds to a distance from the center of the star of $1.85 \cdot 10^{17}$cm. The synthetic spectrum of this model is in close agreement with the observed spectrum of IRC +10216 in the wavelength region between 2μm and 5cm. In the near infrared region shortward of $\lambda \approx 2\mu$m the calculated spectrum decreases too steeply as compared to the observed fluxes. As discussed in Sect. 5.2, this behaviour may be due to the existence of unrealistic large dust particles in the inner part of the dust shell model, which is a result of the assumption of stationarity.

The dependence of the FIR flux on the location of the outer boundary is shown in Fig. 9. The solid line is the same as in Fig. 8 with $R_{max} = 2 \cdot 10^3 R_0$. A reduction of the shell extension to $5 \cdot 10^2 R_0$ leads to a reduction of the FIR flux of the calculated spectrum as indicated by the short-dashed curve (the calculated flux values are multiplied by a factor of 1/16 in order to eliminate the pure geometrical effect). The dotted curve results from a location of the outer boundary at $10^4 R_0$

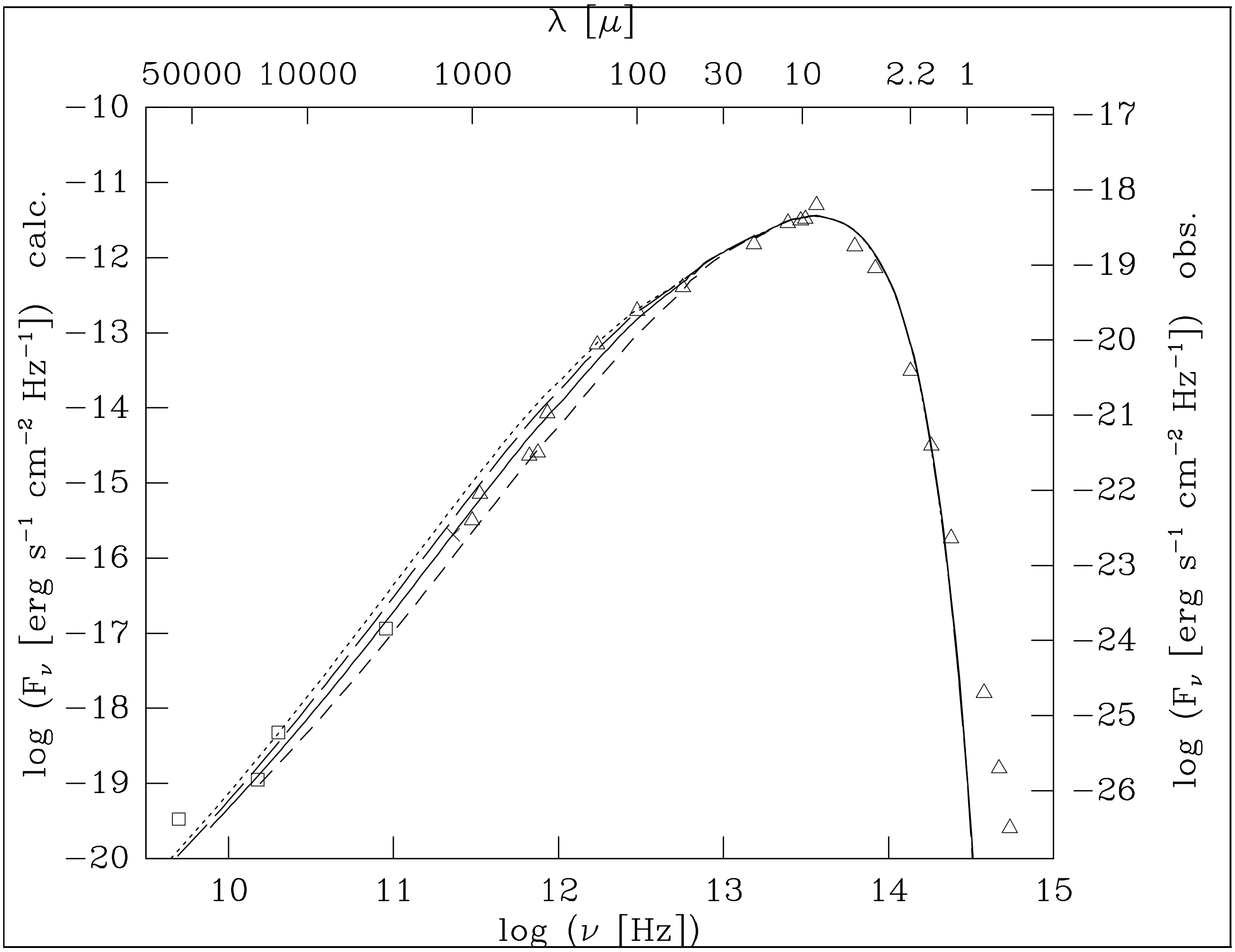

Fig. 9. The effect of varying the location of the outer boundary. Observational data are the same as in Fig. 8. The outer boundary is located at: $5 \cdot 10^2 R_0$ (short-dashed curve, calculated values multiplied by 1/16); $2 \cdot 10^3 R_0$ (solid curve); $5 \cdot 10^3 R_0$ (long-dashed curve, calculated values multiplied by 6.25) and $1 \cdot 10^4 R_0$ (dotted curve, calculated values multiplied by 25). The observed spectrum is best represented for an outer shell boundary located at $2 \cdot 10^3 R_0$ (solid curve).

(the calculated values are increased by a factor of 25) which produces too much flux at wavelengths larger than $\approx 200\mu$m. Thus, the observed mid– and FIR spectrum of IRC +10216 is best reproduced by our model for an outer shell radius of $R_{\max} = 2 \cdot 10^3 R_0$ (cf. Fig. 8).

From CO (2–1) line observations Knapp et al. (1982) and Huggins et al. (1988) find that the CO molecular envelope around IRC +10216 extends out to ~ 3 arcmin. Outside this radius the CO molecule is presumably destroyed via photodissociation by the interstellar radiation field. If the dust shell is even more extended, it is at least optically thin for the CO dissociating UV photons. Since the dust extinction decreases with increasing wavelength, there should be no relevant contribution to the emergent flux by thermal dust emission at FIR wavelengths. Therefore, we consider the measured outer radius of the CO envelope as an upper limit for the relevant extension of the dust shell.

As the stellar luminosity is a physical parameter of our models, we can estimate the distance to IRC +10216. If we assume that there is no interstellar extinction, then the distance d is given by

$$d = R_{\max} \left(\frac{F_{\nu,\mathrm{calc}}(R_{\max})}{F_{\nu,\mathrm{obs}}(d)} \right)^{\frac{1}{2}} \quad . \tag{27}$$

With $R_{\max} = 2 \cdot 10^3 R_0 = 1.85 \cdot 10^{17}$cm, Eq. (27) yields $d \approx 170$pc. Given this distance the measured angular shell extension of $3'$ yields an outer radius of the IRC +10216 envelope of $4.58 \cdot 10^{17}$cm. In our model this corresponds to $R_{\max} = 4.95 \cdot 10^3 R_0$. With this value for the outer boundary (long-dashed curve in Fig. 9), the calculated flux is slightly higher than the observed spectrum at wavelengths longward of $\lambda = 200\mu$m. As the stationary models are likely to overestimate the thermal emission in the outer parts of the shell (Sect. 5.2), this flux deviation should not be attached too much importance to.

The total mass contained in the circumstellar shell results to $M_{\mathrm{CS}} = 0.60 M_\odot$ for $R_{\max} = 2 \cdot 10^3 R_0$ and $M_{\mathrm{CS}} = 0.95 M_\odot$

for $R_{\max} = 5 \cdot 10^3 R_0$, respectively from our calculations. These values imply a mass of the main sequence progenitor of IRC +10216 of $M_{\rm ZAMS} > 1.30 M_\odot$.

The distance of 170pc to IRC +10216 is about 60 per cent smaller than the often quoted value of 290pc suggested by Herbig & Zappala (1970). They assume an absolute bolometric magnitude of $M_{\rm bol} = -7$ ($L_\star = 4.88 \cdot 10^4 L_\odot$) for IRC +10216 and a value for the measured bolometric flux of $2 \cdot 10^{-12}\,{\rm Wcm}^{-2}$. However, it is not clear at which phase of the light curve this value is obtained. The distance to IRC +10216 of 170pc as derived from our synthetic spectrum, on the other hand, is in rather good agreement with the value of $\approx$ 150pc which was first suggested by Zuckerman et al. (1986) and has recently been supported by Kastner (1992).

5.5.3. Spatial intensity distribution

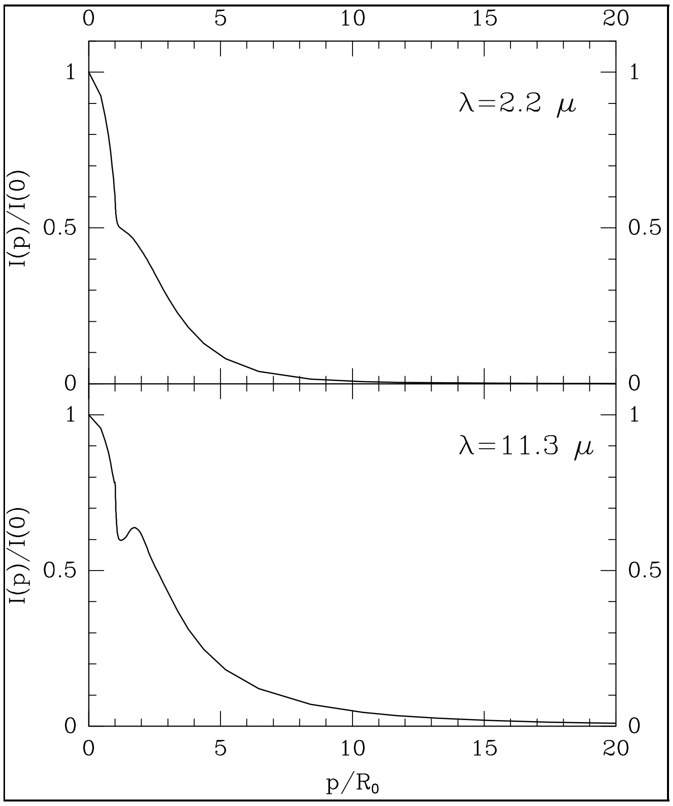

Fig. 10. Calculated spatial brightness distribution at the outer shell boundary. Upper diagram: $\lambda = 2.2\mu$m, lower diagram: $\lambda = 11.3\mu$m

In Fig. 10 the calculated center-to-limb variation of the specific intensity is shown at the outer boundary of the dust shell at two different wavelengths. Besides the main maximum at the center, a pronounced secondary maximum of the emergent 11μm intensity is seen at a radial offset of $\approx 2R_0$, which is caused by thermal dust emission in the dense inner region of the dust shell. Due to the larger optical depth at 2.2μm ($\tau_{2.2\mu} = 6.05$, $\tau_{11.3\mu} = 1.31$), the spatial intensity distribution at this shorter wavelength merely exhibits a plateau-like structure around $2R_0$.

At a distance of 170pc, this striking intensity structure would subtend an angular region of $\approx 0.15''$ diameter, which is too small to be directly resolved with current IR-telescopes. Interferometric observations of IRC +10216 have been performed by several authors at different wavelengths (eg. $1.6 - 4.8\mu$m (Dyck et al. 1984); $1.6 - 5\mu$m (Ridgway & Keady 1988); $2.2 - 20\mu$m (McCarthy et al. 1980); 2μm and 11μm (Dyck et al. 1987); 11μm (Sutton et al. 1979; Danchi et al. 1990)). These observations reveal an asymmetric spatial structure of the source at wavelengths shorter than 5μm (Dyck et al. 1984; Dyck et al. 1987; McCarthy et al. 1980; Ridgway & Keady 1988) while in the 10μm region no major asymmetries are found (Dyck et al. 1987; Sutton et al. 1979). A temporal variation of the visibility data with the phase of the light curve is also seen at 2.2μm (Dyck et al. 1984), 5μm (McCarthy et al. 1980) and at 11μm (Danchi et al. 1990).

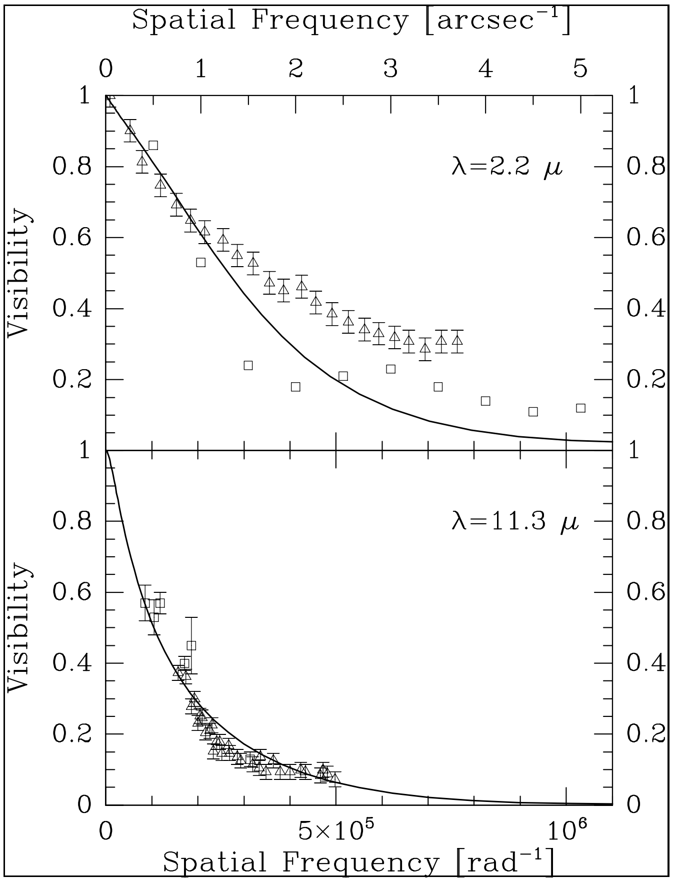

Fig. 11. Calculated visibility (solid lines) at 2.2μm (upper diagram) and 11.3μm (lower diagram) compared with the interferometric observations of: Ridgway & Keady (1988) (□, N-S scan) and Dyck et al. (1984) (△, E-W scan) at 2.2μm (upper diagram) and of McCarthy et al. (1980) (□, at 10.2μm, 11.1μm and 12.5μm) and of Sutton et al. (1979) (△) at 11.1μm (lower diagram). All observed values are obtained near maximum light.

In Fig. 11 we present the calculated visibility of our model at $\lambda = 2.2\mu$m (upper diagram) and $\lambda = 11.3\mu$m (lower diagram) together with the corresponding visibility data observed near the maximum of the 2.2μm light curve. In the 10μm region we find a reasonable agreement between calculated and observed visibility. The agreement between calculated and observed visibilities at 2.2μm, however, is less satisfactory. This may be due to the fact, that our model is spherically symmetric, whereas the observations indicate an asymmetric shape of the IRC +10216 shell at this wavelength. However, it should be noted that our result is much closer to the observed 2.2μm visibility than the model of Martin & Rogers (1987). In their model, the emergent intensity at 2.2μm drops by a factor of ≈ 30 at the outer edge of the central star which produces high values of the visibility at high spatial frequencies. They obtain a considerable improvement between observed and calculated values by a "flat interpolation through the central region" of the emergent 2.2μm intensity.

In order to calculate the theoretical fringe visibilities from the spatial intensity distribution, the radial coordinate has to be converted to an angular separation from the center of the star. For the results shown in Fig. 11 we had to assume a distance of 140pc to IRC +10216, which is about 20% less than the value derived from the spectrum. Although both values are in reasonable agreement, this difference in the derived distance values may point at a problem of our treatment of grain condensation by classical nucleation theory. In our models the nucleation of dust grains starts at rather high temperatures of ≈ 1400K i.e. relatively close to the photosphere. Theoretical investigations of the more realistic microscopic treatment of grain formation by calculating the chemical pathway indicate, that carbon grains should form at a lower temperature around ≈ 1000K (Keller 1987; Gail & Sedlmayr 1987a; Cherchneff et al. 1992) and, thus, at a larger distance from the star. This would lead to a more extended intensity distribution and thus to more strongly peaked visibility curves at small spatial frequencies. In other words: if the onset of grain nucleation would take place at a larger separation from the star, we had to assume a larger distance to the star in order to obtain the same fit to the observed values as shown in Fig. 11. In order to retain the distance of 170pc, the onset of dust formation has to be shifted outwards by a factor of 1.2 to a location at around $1.7 R_0$.

5.5.4. The final outflow velocity

As already mentioned above, the terminal velocity $v_\infty = 20.7\,\mathrm{kms}^{-1}$ resulting from the model calculation presented here is significantly higher than the value of $\approx 14 - 15\,\mathrm{kms}^{-1}$ observed for IRC +10216 (e.g. Olofsson et al. (1993)).

The terminal outflow velocity resulting from the model calculations can effectively be reduced by reducing the carbon abundance ϵ_C (cf. Sect. 5.3). A model fixed by the same mass–loss rate $\dot{M} = 8 \cdot 10^{-5} M_\odot/\mathrm{yr}$, luminosity $L_\star = 2.4 \cdot 10^4 L_\odot$, and stellar mass $M_\star = 0.7 M_\odot$, but with a reduced carbon to oxygen ratio of e.g. $\epsilon_\mathrm{C}/\epsilon_\mathrm{O} = 1.25$ yields a terminal velocity of $v_\infty = 14.4\,\mathrm{kms}^{-1}$. A reduction of ϵ_C however, simultaneously leads to a significant "blue shift" of the emergent spectrum (cf. Sect. 5.3), which would no longer match the observed energy distribution of IRC +10216. Thus, in order to compensate for this effect, we additionally have to reduce the stellar luminosity $L_\star$ and/or to increase the mass–loss rate $\dot{M}$, which both would lead to a "red shift" of the spectrum (cf. Sect. 5.3).

An alternative model, which also would fit the individual observations of IRC +10216 reasonably well is fixed by the set of parameters $M_\star = 0.7 M_\odot$, $L_\star = 2.3 \cdot 10^4 L_\odot$, $\dot{M} = 8 \cdot 10^{-5} M_\odot/\mathrm{yr}$, $\epsilon_\mathrm{C}/\epsilon_\mathrm{O} = 1.30$. This model yields a terminal velocity of $16.6\,\mathrm{kms}^{-1}$, a spectrum very similar to the one presented in Fig. 8 and also visibilities very similar to those depicted in Fig. 11. For the alternative model we derive a distance to IRC +10216 from the measured flux again of $d \approx 170$pc but a value of $d \approx 120$pc from the measured visibilities and, thus, obtain an inconsistency of about 40% between both distances derived for the same object. Therefore, and for the reason given below, we have chosen to put up with the too high value of the terminal velocity.

The main problem of our present approach of course is the application of a stationary model for the interpretation of pulsating objects. As discussed in Sects. 5.1 and 5.2, this assumption leads to the formation of unrealistic large particles in the region around the sonic point, which absorb radiative momentum less effectively than the same amount of dust contained in small particles would do. In order to surmount the Eddington limit (Eq. (24)), i. e. in order to provide the energy, necessary to lift the material out of the stars gravitational field, therefore, a larger amount of condensed material is needed if the grains are large compared to the typical wavelength of the radiation field. In the models, this larger degree of condensation can be achieved by increasing the carbon abundance over the value needed for small particles to drive the wind. The higher degree of condensation, however, also leads to a more effective acceleration of the wind in the region outside the sonic point and, thus, to higher terminal velocities (cf. Sect. 5.3).

In the real pulsating objects two effects are present, which are in favour for smaller outflow velocities:

i) the particles remain smaller (cf. Sect. 5.2) and

ii) the dissipation of shock wave momentum supports the levitation of the material out of the gravitational field, i.e. a smaller contribution of radiative acceleration is needed in the inner shell region to separate the material from the star.

In fact, the dynamical calculations of Fleischer et al. (1992) for dust forming shells around long–period variable stars yield lower terminal wind velocities as do the stationary models presented here. Detailed radiative transfer calculations in these time dependent models are presently beeing performed. The results will be presented in a forthcoming paper.

6. Conclusions

We have calculated self-consistent models of spherically symmetric, stationary dust-driven winds around cool carbon stars. These models include a detailed treatment of hydrodynamics, thermodynamics, chemistry, dust formation and –growth and of the radiative transfer problem. In this approach, the structure of the dust shell is completely fixed by four parameters: stellar mass $M_\star$, stellar luminosity $L_\star$, mass-loss rate $\dot{M}$ and the initial element composition of the gas ϵ_i.

The transport coefficients of the dust grains are calculated by means of Mie theory for homogeneous spherical particles of arbitrary size, taking explicitly into account the resulting local size distribution function of the dust grains.

Our results imply, that in a stationary dust-driven wind the common assumption of the small particle approximation for calculating the transport coefficients of the dust component is not justified. Especially in the inner region of the dust envelope, where the mass outflow is generated by radiation pressure on dust grains, the dust opacity and, thus, the radiative force acting on the grains, is essentially reduced by the presence of the large particles.

The theoretical spectra produced by the dust shell models are in agreement with the FIR observations of cool carbon-rich

AGB objects. The calculated spectra are sensitive to variations of the mass-loss rate, the stellar luminosity and the initial carbon abundance. Within the range of stellar masses, for which purely dust-driven winds exist for reasonable values of the stellar luminosity, the calculated spectra are almost independent of the stellar mass.

In the NIF spectral region the response of the calculated colour indices to changes of the stellar parameters is in qualitative agreement with the observed colour indices. The absolute values of the theoretical colour indices, however, deviate in a systematic way from the observations. This deviation might be a consequence of our stationary approach. The assumption of stationarity results in the formation of rather large dust grains in the circumstellar shell. As the real dust forming objects are mainly pulsating variables, the formation of very large grains is prevented by the limitation of the time available for grain growth due to significant periodic changes of the hydrodynamical and thermodynamical conditions in the dust forming region. Thus, for a quantitative reliable calculation of the NIF spectra the effects of pulsation have to be taken into account. Investigations with regard to a dynamical modelling are currently under way. Based on the time–dependent model calculations of Fleischer et al. (1992) for circumstellar dust shells around long–period variables, Winters et al. (1994) have calculated the synthetic lightcurves of these models. A detailed discussion of the complete resulting spectra will be subject to a forthcoming paper.

Applying the stationary model calculations to IRC +10216, we find reasonable agreement with the observed energy distribution and the observed interferometric data obtained at light maximum for a model which is fixed by a stellar mass $M_\star = 0.7 M_\odot$, a stellar luminosity $L_\star = 2.4 \cdot 10^4 L_\odot$, a mass-loss rate $\dot{M} = 8 \cdot 10^{-5} M_\odot \mathrm{yr}^{-1}$ and a carbon to oxygen ratio $\epsilon_\mathrm{C}/\epsilon_\mathrm{O} = 1.40$. From the energy distribution of this model we obtain a distance to IRC +10216 of $d = 170$pc and a mass contained in the circumstellar shell of $0.6 M_\odot \leq M_\mathrm{CS} \leq 0.95 M_\odot$.

The comparison between observed and calculated visibilities yields a distance of $d = 140$pc. This difference may result from our treatment of carbon grain condensation by classical nucleation theory, which leads to the formation of grains already at relatively high temperatures and, thus, close to the stellar photosphere. A larger separation of the grain formation zone from the photosphere, as is expected if carbon grain condensation proceeds via the formation of PAH's, possibly could resolve this problem.

Despite of the shortcomings mentioned above, which are largely due to the application of stationary theoretical models to in reality pulsating objects, we achieve satisfactory agreement with important observational results by applying a self-consistent model which involves only the four fundamental parameters.

Acknowledgements We are grateful to the referee, Dr. M. Guelin, whose comments have helped to improve the paper. J.M.W. thanks A.J. Fleischer for many discussions and useful suggestions. This work has partly been supported by the Deutsche Forschungsgemeinschaft, DFG-Schwerpunkt: "Theorie kosmischer Plasmen" (grant Se 420/4-3).

A. Determination of stellar temperature and stellar radius

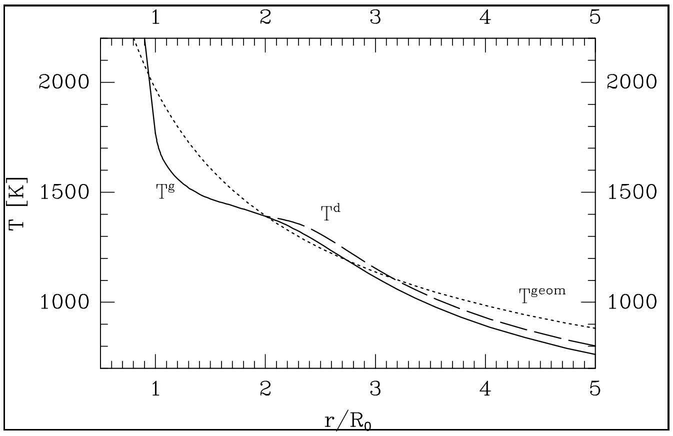

Fig. 12. Radial variation of gas temperature T^g (solid line), size-independent dust temperature T^d (dashed line) and the temperature resulting from a geometrically diluted radiation field T^{geom} (dotted line).

Table 2. Possible values for stellar temperature and stellar radius in the converged model

$R_\star/R_0$	$T_\star$/K	τ_L	$\tau_{1\mu}$	$\tau_{10\mu}$	τ_R
0.96	2008	4.23	23.1	5.27	4.13
2.02	1387	1.29	19.1	1.20	0.14
2.75	1189	1.12	17.0	0.85	0.08
3.16	1108*	0.83	15.5	0.75	0.07
128	175*	0.01	0.35	0.02	0.001
1.00	1971	2/3	—	—	2.94

* refers to the dust temperature

starting model: $R_{\star,0} = 9.25 \cdot 10^{13}\mathrm{cm} = R_0$

In the case of a spherically extended stellar atmosphere, composed of the "stellar photosphere" and a circumstellar shell, it is not a priori obvious how to define the so called "basic stellar parameters" *effective (or stellar) temperature* and *photospheric (or stellar) radius* (cf. Baschek et al. 1991). The virtual relevant physical quantity in this context is the energy released in the stellar interior and subsequently transported through the outer layers of the star. A physically meaningful determination of the stellar temperature and the stellar radius is then based on the Stefan–Boltzmann law from the requirement that the local temperature equals $(L_\star/4\pi\sigma r^2)^{1/4}$ at a certain radial distance $r = R_\star$. However, this is only possible if the temperature stratification of the atmosphere is already known, e.g. from a model calculation. In order to calculate the model atmosphere, on the other hand, one has to prescribe four parameters which characterize the star. The classical choice for this parameter set is of course the quadruple ($M_\star$, $L_\star$, $T_\star$, ϵ_i). But then the problem arises, how to force the resulting local temperature to match the stellar temperature at the radius $R_\star$ which, for given $L_\star$ and $T_\star$ is uniquely determined from Stefan–Boltzmann's law. This problem is usually solved by prescribing additionally (and somewhat arbitrary in the case of a non-grey atmosphere) a certain value of some optical depth to be reached at $R_\star$.

Based on a two stream approximation for the specific intensity, Lucy (1971) obtains a closure relation for the moment equations of the radiation field. In the case of radiative equilibrium this approximation leads to a semi-analytical expression for the temperature structure (Lucy 1976):

$$T^4(r) = \frac{1}{2}T_\star^4\left[1-\sqrt{1-\left(\frac{R_\star}{r}\right)^2}+\frac{3}{2}\tau_{\rm L}(r)\right]\frac{\kappa_{\rm J}}{\kappa_{\rm P}} \qquad \text{(A1)}$$

with the geometrically diluted optical depth $\tau_{\rm L}$ defined by the differential equation

$$\frac{d\tau_{\rm L}}{dr} = -\left(\frac{R_\star}{r}\right)^2\chi_{\rm H}(r) \qquad \text{(A2)}$$

with the boundary condition

$$\tau_{\rm L}(r\rightarrow\infty) = 0\ . \qquad \text{(A3)}$$

The value of the stellar radius $R_\star$ then follows from the consistency condition $T(R_\star) = T_\star$ which in terms of Eq. (A1) requires

$$\tau_{\rm L}(R_\star) = \frac{2}{3}\left[2\frac{\kappa_{\rm P}}{\kappa_{\rm J}}-1\right]\ . \qquad \text{(A4)}$$

As Eq. (A4) is a second boundary condition to the first order differential equation (A2), the stellar radius becomes an Eigenvalue of Eq. (A2). Since the stellar radius on the other hand is uniquely determined by the Stefan–Boltzmann law for given stellar temperature and stellar luminosity, Eq. (A4) can be used to calculate another unknown quantity as an Eigenvalue of the equation system which describes the CDS. This method is used in grey approximation to fix the mass-loss rate as the Eigenvalue in our initial models. The stellar radius of the initial model subsequently serves as the normalization constant R_0. The two-stream approximation, however, is only justified in an optically thin atmosphere. In the case of an optically thick atmosphere, therefore, the temperature has to be calculated from a detailed treatment of the radiative transfer problem. From the given starting model, we consider the mass-loss rate as a parameter of the equation system instead of $T_\star$, stellar temperature and stellar radius are then not longer needed in order to fix the solution. If a value of $T_\star$ is required for some purpose (e.g. for the location of the model in the HR diagram) it can be obtained from the converged model via the Stefan–Boltzmann law. In Fig. 12 the kinetic gas temperature $T^{\rm g}$, the size-independent dust temperature $T^{\rm d}$ and the temperature which results from a geometrically diluted radiation field $T^{\rm geom} = (L_\star/4\pi\sigma r^2)^{1/4}$ are shown for the model discussed in Sect. 5.5. The possible determinations of $R_\star$ and $T_\star$ are summarized in Tab. 2 together with the values of different optical depths at the respective radii.

References

Allen C.W., 1973, Astrophysical Quantities. The Athlone Press, London

Barnbaum C., Kastner J.H., Zuckerman B.: 1991, AJ, 102, 289

Baschek B., Scholz M., Wehrse R., 1991, A&A, 246, 374

Beck H.K.B., Gail H.-P., Henkel R., Sedlmayr E., 1992, A&A, 265, 626

Berruyer N., Frisch H., 1983, A&A, 126, 269

Bowen G.H., 1988, ApJ, 329, 299

Cherchneff I., Barker J.R., Tielens A.G.G.M., 1992, ApJ, 401, 269

Danchi W.C., Bester M., Degiacomi C.G., McCullough P.R., Townes C.H., 1990, ApJ, 359, L59

Dominik C., Gail H.-P., Sedlmayr E., 1989, A&A, 223, 227

Dominik C., Gail H.-P., Sedlmayr E., Winters J.M., 1990, A&A, 240, 365

Dyck H.M., Zuckerman B., Howell R.R., Beckwith S., 1987, PASP, 99, 99

Dyck H.M., Zuckerman B., Leinert C., Beckwith S., 1984, ApJ, 287, 801

Epchtein N., Le Bertre T., Lépine J.R.D, 1990, A&A, 227, 82

Fleischer A.J., Gauger A., Sedlmayr E., 1991, A&A, 242, L1

Fleischer A.J., Gauger A., Sedlmayr E., 1992, A&A, 266, 321

Frantsman Y.L., Eglitis I.E., 1988, SvA, 14, L109

Gauger A., Gail H.-P., Sedlmayr E., 1990, A&A, 235, 245

Gail H.-P., Sedlmayr E., 1984, A&A, 132, 163

Gail H.-P., Sedlmayr E., 1985, A&A, 148, 183

Gail H.-P., Sedlmayr E., 1987a, Dust Formation in Stellar Winds. In: Morfill, G.E., Scholer, M. (eds.) Physical Processes in Interstellar Clouds. NATO ASI series C, Reidel, Dordrecht, p. 275

Gail H.-P., Sedlmayr E., 1987b, A&A, 171, 197 (Paper III)

Gail H.-P., Sedlmayr E., 1988, A&A, 206, 153

Gail H.-P., Keller R., Sedlmayr E., 1984, A&A, 133, 320

Goebel J.H., Moseley S.H., 1985, ApJ, 290, L35

Gow C.E., 1977, PASP, 89, 510

Habing H.J., 1990, The Evolution of Red Giants to White Dwarfs, a Review of the Observational Evidence. In: Mennessier M.O., Omont A. (eds.) From Miras To Planetary Nebulae: Which Path for Stellar Evolution. Editions Frontières, Gif sur Yvette Cedex, p. 16

Herbig G.H., Zappala R.R., 1970, ApJ, 162, L15

Holzer T.E., MacGregor K.B., 1985, Mass Loss Mechanisms for Cool, Low-Gravity Stars. In: Morris M., Zuckerman B. (eds.) Mass Loss from Red Giants. Reidel Publishing Company, p. 229

Huggins P.J., Olofsson H., Johansson L.E.B., 1988, ApJ, 332, 1009

Jura M., 1983a, ApJ, 267, 647

Jura M., 1983b, ApJ, 275, 683

Jura M., 1986a, ApJ, 303, 327

Jura M., 1986b, Ir. Astron. J., 17, 322

Kastner J.H., 1992, ApJ, 401, 337

Keller R., 1987, Polyaromatic Hydrocarbons and the Condensation of Carbon in Stellar Winds. In: Léger A., d'Hendecourt L., Boccara N. (eds.) Polycyclic Aromatic Hydrocarbons and Astrophysics. NATO ASI series C, Reidel, Dordrecht, p. 387

Keller R., Sedlmayr E., 1983, Mitt. Astron. Ges., 60, 312

Knapp G.R., 1986, ApJ, 311, 731

Knapp G.R., Morris M., 1985, ApJ, 292, 640

Knapp G.R., Philips T.G., Leighton R.B., et al., 1982, ApJ, 252, 616

Kozasa T., Hasegawa H., Seki J., 1984, Ap&SS, 98, 61

Krüger D., Gauger, A., Sedlmayr E., 1994, A&A, submitted

Kwok S., 1975, ApJ, 198, 583

Lafon J.-P.J, Berruyer N., 1991, A&AR, 2, 249

Lambert D.L., Gustafsson B., Eriksson K., Hinkle K.H., 1986, ApJS, 62, 373

Le Bertre T., 1987, A&A, 176, 107
Léger A., Puget J.L., 1984, A&A, 137, L5
Lucy L.B., 1971, ApJ, 163, 95
Lucy L.B., 1976, ApJ, 205, 482
Mamon G.A., Glassgold A.E., Huggins P.J., 1988, ApJ, 328, 797
Maron N., 1990, Ap&SS, 172, 21
Martin P.G., Rogers C., 1987, ApJ, 322, 374
McCarthy D.W., Howell R., Low F.J., 1980, ApJ, 235, L27
Menietti J.D., Fix J.D., 1978, ApJ, 224, 961
Mihalas D., 1978, Stellar Atmospheres. 2nd. ed., W.H. Freeman & Co., San Francisco
Olofsson H., Eriksson K., Gustafsson B., Carlström U., 1993, ApJS, 87, 267
Orofino V., Colangeli L., Bussoletti E., Blanco A., Fonti S., 1990, A&A, 231, 105
Ridgway S.T., Keady J.J., 1988, ApJ, 326, 843
Sahai R., Claussen M.J., Masson C.R., 1989, A&A, 220, 92
Salpeter E.E., 1974, ApJ, 193, 585
Schönberner D.: 1983, ApJ, 272, 708
Scholz M., Tsuji T., 1984, A&A, 130, 11
Schutte W.A., Tielens A.G.G.M., 1989, ApJ, 343, 369
Sedlmayr E., Winters J.M., 1991, Dust in the Shells of Cool Giants and Supergiants. In: Crivellari L., Hubeny I., Hummer D.G. (eds.) Stellar Atmospheres: Beyond Classical Models. NATO ASI series C, Kluwer Academic Publishers, Dordrecht, p. 397
Sopka R.J., Hildebrand R., Jaffe D.T., et al., 1985, ApJ, 294, 242
Sutton E.C., Betz A.L., Storey J.W.V., Spears D.L., 1979, ApJ, 230, L105
Treffers R., Cohen M., 1974, ApJ, 188, 545
van der Veen W.E.C.J., Habing H.J., 1988, A&A, 194, 125
van der Veen W.E.C.J., Rugers M., 1989, A&A, 226, 183
Walmsley C.M., Chini R., Kreysa E., et al., 1991, A&A, 248, 555
Wickramasinghe N.C., Donn B.D., Stecher T.P., 1966, ApJ, 146, 590
Winters J.M., Fleischer A.J., Gauger A., Sedlmayr E., 1994, A&A, submitted
Witteborn F.C., Strecker D.W., Erickson E.F., et al., 1980, ApJ, 238, 577
Zuckerman B., Dyck H.M., Clausen M.J., 1986, ApJ, 304, 401

This article was processed by the author using Springer-Verlag LaTeX A&A style file 1990.